https://doi.org/10.5194/egusphere-2025-6395
Preprint. Discussion started: 23 January 2026
© Author(s) 2026. CC BY 4.0 License.

Quantifying Water Vapor Age: A Dynamical Constraint on the Response of the Global Water Cycle to Climate Change

Philippe Boulanger[1,2] and Robert Fajber[1,2]
[1]Department of Atmospheric and Oceanic Sciences, McGill University, Montreal, Québec Canada
[2]Brace Water Center, McGill University, Ste Anne de Bellevue, Québec Canada
Correspondence: Philippe Boulanger (philippe.boulanger@mail.mcgill.ca)

Abstract. One important uncertainty of climate change is the rate of acceleration of the global water cycle. While the Clausius-Clapeyron equation predicts a 7% rise in atmospheric moisture per degree of warming, climate models suggest globally averaged precipitation only changes by 1% to 3% (the hydrologic sensitivity). This discrepancy can be explained by a 4% to 6% increase in water vapor (WV) age per degree of warming. Typically, changes in precipitation are used to calculate changes in WV age by assuming a well-mixed atmosphere to calculate a global value, which obscures the effects of regional dynamics on changes to the WV age spectrum. In this work, we have developed novel passive tracers for calculating the WV age spectrum in an Eulerian model. By directly simulating the moments of the WV age spectrum, our method resolves the temporal and spatial variability of the WV age distribution, and allows us to calculate the age spectrum of the precipitating water as well. We have demonstrated our technique by implementing these tracers in the Isca modelling framework using a quasi-realistic configuration which we then perturbed with global sea surface temperature anomaly experiments. In our control experiment, the globally averaged mean WV age and mean age of precipitation was 7.06 and 7.33 days respectively, and compared well to previous estimates using Lagrangian models. With climate change, WV age generally increased in the troposphere and decreased in the stratosphere. Globally, the mean WV age increased by $4.93\% K^{-1}$ and the age of precipitation increased by $3.16\ \% K^{-1}$. With our temporal and spatial resolution of WV age, we also resolve the effects of the Hadley cell strengthening, as well as the poleward shift and intensification of the midlatitude eddies and storm tracks, demonstrating how the regional changes in WV age differed from the regional changes in precipitation age.

1 Introduction

The impact of climate change on the water cycle is frequently quantified through the hydrologic sensitivity, which is defined as the change in global average precipitation relative to the change in average surface temperature. While the Clausius-Clapeyron equation predicts a 7% rise in atmospheric moisture per degree of warming, climate models suggest that hydrologic sensitivity, is only 1% to 3%. This discrepancy can be explained by a 4% to 6% increase in water vapor (WV) age per degree of warming

https://doi.org/10.5194/egusphere-2025-6395
Preprint. Discussion started: 23 January 2026
© Author(s) 2026. CC BY 4.0 License.

(Gimeno et al., 2021). Understanding the controls on the hydrologic sensitivity is an important area of current climate research, as the spread in climate models is still quite large (Pendergrass, 2020).

Most calculations of WV age use indirect methods (Bonan et al., 2024; Ayantobo and Wei, 2025). These methods postulate that the global turnover time (TUT), defined as the mean age of precipitation, is equal to the ratio of the globally averaged precipitable water (W) to the globally averaged precipitation rate (P) (Trenberth, 1998),

$$\mathrm{TUT} = \frac{\langle \overline{W} \rangle}{\langle \overline{P} \rangle}, \tag{1}$$

where $\langle \cdot \rangle$ denotes the global average and $\overline{\cdot}$, the time average. It is also used as a proxy for the globally averaged mean WV age. In these calculations, precipitation is either calculated directly from diagnostics, or approximated by the water mass flux (Held and Soden, 2006). For example, Sodemann (2020) and Trenberth (2011) calculated TUT as 8.48 days and 9.3 days respectively. Using an idealized aquaplanet model, O'Gorman and Schneider (2008) calculated that TUT increases by about 3.8% per degree of warming, which sits in the 3.5 to 5.5% range reported in Gimeno et al. (2021). In Held and Soden (2006), they assume that precipitation changes in the tropics are the main driver of changes in TUT. However, it is not obvious why precipitation changes should constrain WV age changes, and not the other way around. Futhermore, this global average of the mean WV age cannot resolve the effects of the atmospheric circulation on the mean WV age which limits our ability to properly understand the relationship between WV age, moisture and precipitation.

To investigate the effects of different modes of WV transport on the WV age spectrum, let us define the shape parameter of the distribution as

$$s = \frac{\tau}{\sigma}, \tag{2}$$

where τ is the mean and σ is the standard deviation of the WV age distribution. If we consider WV travelling via a strong and dominant transport pathway (large red arrows on figure 1), the WV will age collectively as it travels between point A and B. Then, s will be greater than 1 and the distribution will be approximately gaussian at its destination. On the other hand, if it can travel via a multitude of pathways like between point A and C (small blue arrows), the age will be more varied at arrival. Then, s will be lower than 1, and the distribution exponential. Suppose some transport pathway were to be modified by climate change. The red arrow on figure 1 could be modified, and the WV age distribution in point B could be greatly altered. On the other hand, if one out of many the blue arrows were to change, the distribution in point C could see no effective change. The response of the water cycle to climate change is expected to differ depending on the region (Allan et al., 2020), and, by extension, on the changes in WV transport. Therefore, it is considered important to spatially resolve WV age and its distribution (Sodemann, 2020).

Previously, Lagrangian methods have been used to obtain a spatial resolution of the WV age distribution. They report globally averaged values of the mean WV age ranging between 4-5 days (Läderach and Sodemann, 2016) and 8-10 days (Numaguti,

https://doi.org/10.5194/egusphere-2025-6395
Preprint. Discussion started: 23 January 2026
© Author(s) 2026. CC BY 4.0 License.

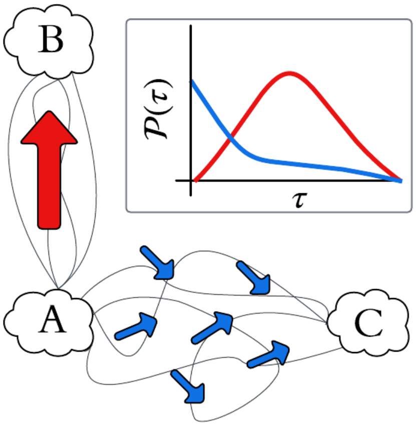

Figure 1. Sketch of the impact of dominant (red) and varied (blue) transport pathways on the shape of the WV age distribution. Black lines are sample pathways that the WV could take between the points.

1999; Tuinenburg and van der Ent, 2016). This unusual outlier of 4-5 days is argued to be due to less realistic moisture transport processes (Tuinenburg and van der Ent, 2016). In a Lagrangian experiment, WV can only be tracked for a fixed amount of time. Although this time frame is optimized (Nieto and Gimeno, 2019), WV that spends multiple months in the atmosphere is not tracked during its entire life cycle, usually at most 10 to 30 days (Nieto and Gimeno, 2019; Tuinenburg and van der Ent, 2016). Although this represents a small portion of the moisture in the atmosphere, it can heavily impact the tail of the WV age distribution. Furthermore, these offline calculations require large amounts of high frequency three dimensional wind data to be saved, which can be computationally expensive.

In this study, we derive and implement passive tracers to track the moments of the WV age distribution in an Eulerian model. This allows us to temporally and spatially resolve the WV age distribution and track its evolution with climate change as online calculations in a global circulation model (GCM). The mean age of precipitation (ν) is also calculated from the WV age. The tracers are validated by implementing them into the Isca modeling framework using a quasi-realistic configuration which we then perturb with global sea surface temperature (SST) anomaly experiments, described in the next section.

We start by presenting the theory behind WV age tracers in section 2.1. We then explain how this method was implemented into the Isca model in section 2.2. The parametrization of the distribution by the Gamma distribution is subsequently detailed in section 2.3. To round up the section 2, our process to calculate the age of precipitation is presented in section 2.4. Later on, we present and analyze the results of the control experiment in section 3.1. It is followed by a similar analysis of the climate change experiment in section 3.2. Finally, the implication of the results from the control and climate change experiment are discussed in section 4.

2 Methods

2.1 Age distribution of a water vapor age tracer

Table 1 summarizes the notation and naming convention that is used in our study, although, we note that studies utilizing different methods have also used some of the same terminology (Gimeno et al., 2021; Tuinenburg and van der Ent, 2016, 2019). We define the WV age, as the time elapsed since evaporation. Now, if we consider an atmospheric parcel, it will have an age distribution associated with the different amounts of water vapor evaporated at different times. We define the age of precipitation as the age of the WV associated with the precipitation that reaches the surface. We denote the mean age of the WV age distribution as τ, and the mean age of precipitation as ν.

Table 1. Notations and naming conventions in the present paper.

Symbol	Description
λ	Longitude.
ϕ	Latitude.
p	Pressure.
$\overline{A}$	Time average of A.
$\{A\}$	Vertical integral of A.
$[A]$	Zonal average of A.
$\langle A\rangle$	Global average (time, zonal and longitudinal) of A.
$q(\lambda,\phi,p)$	Specific humidity $[kg\cdot kg^{-1}]$.
$W(\lambda,\phi)=\{q\}$	Precipitable water vapor $[kg\cdot m^{-2}]$.
$P(\lambda,\phi)$	Precipitation rate $[mm\cdot day^{-1}]$
$a(\lambda,\phi,p)$	Water vapor age $[day]$.
$\tau(\lambda,\phi,p)$	Mean water vapor age $[day]$.
$\nu(\lambda,\phi)$	Mean age of precipitation $[day]$: mean age of the water vapor associated with the precipitation that reaches the surface.

The review paper by Gimeno et al. (2021) introduces some terminology, which Table 2 clarifies in the context of our paper. Although, in Table 2, backward transit time (BTT) is identical in definition to WV age, in practice, BTT is capped by the integration time of Lagrangian experiments. Therefore, the lifetime distribution should differ from our WV age distribution. In this context, theoretically identical quantities can have different behavior in practice. We think that these differences are important to keep in mind when comparing results of indirect methods, Lagrangian experiments and Eulerian calculations.

We will now derive an evolution equation to track the age distribution of the specific humidity tracer, q. The sources and sinks of q are evaporation (E) and a general sink term S^{-}, which regroups negative moisture tendencies from the condensation

https://doi.org/10.5194/egusphere-2025-6395
Preprint. Discussion started: 23 January 2026
© Author(s) 2026. CC BY 4.0 License.

Table 2. Definitions from Gimeno et al. (2021) and their equivalents in our study.

Term	**Definition by Gimeno et al. (2021)**	**Our Equivalent**
Turnover Time (TUT)	Bulk mean age of the outflow from a reservoir. It equals the global average mean age of precipitation.	Temporal and global average mean age of precipitation, $\langle \nu \rangle$.
Backward transit time (BTT) or lifetime	Time that a precipitated water particle spent in the atmosphere.	WV age (τ) at the time of precipitation.
Lifetime distribution (LTD)	The probability density function of all lifetimes or BTT in a specific region or globally. The global precipitation-weighted average of LTD is equal to TUT.	Water vapor age distribution in the same specific region or globally.
Forward transit time (FTT)	The time that an evaporated water particle will spend in the atmosphere. Globally averaged, it is equal to BTT, but presents different regional patterns.	No direct equivalent in our calculation, but globally averaged, should equal the mean WV age.

and convection schemes within a climate model. For WV injected into the system at time t_e, the age is given by $a = t - t_e$. If we define the age concentration of the amount of WV q as q_a so that $q_a da$ is the amount of WV with age between $(a, a + da)$, then at any given moment in time, the WV content associated with that age category is $q(t_e = t - a)$, i.e.

$$q_a(t)da = q(t, t_e = t - a)dt. \tag{3}$$

Then, based on Fajber and Kushner (2021), we can find an evolution equation for q_a by considering that at each time step, aging will occur, causing q_a to be associated with the moisture content of one time step forward. Then the evolution equation for q_a is

$$\frac{\partial q_a}{\partial t} + \nabla \cdot \mathbf{v} q_a = E + \frac{q_a}{c} S^- - \frac{\partial q_a}{\partial a}, \tag{4}$$

where E and S^- are instantaneous sources and sinks of WV. This is similar to the Green's function method (Orbe et al., 2016; Hall and Plumb, 1994), which has been used to track the age distribution of tracers (Éric J.M Delhez and Éric Deleersnijder, 2002). This method quantifies the response of the system to an infinitesimal impulse tracer, injected into the system by E in our case. At each time step, the evolution equation applied to the solution of the Green's function is the instantaneous injection by E. If we solve for the solution of the Green's function for every point and every time step, we can recover the age distribution of the tracer everywhere exactly as it is affected by some sinks, S^-, and transport. Directly implementing this type of tracer that tracks the entire distribution of ages requires initializing new tags at every time step and is very computationally expensive. In practice, the pulses are released only a handful of times, and averaged over a limited region. We have similar issue here, where we would need to initialize tracers for q_a at each time step. Our solution to this problem is to track the moments of the distribution. In applications of the Green's function method, the temporal and spatial resolution is compromised at the profit of tracking the entire distribution. Instead of discretizing in time as with the Green's function method, we are using a method of moments (Éric J.M Delhez and Éric Deleersnijder, 2002). We argue that it is both computationally convenient and mathematically efficient to approximate the full distribution using the first n moments as opposed to estimating it using n tracers launched at different times. The full equations are derived in Appendix A, but we briefly summarize the development here. The n-th normalized moment of the normalized age distribution, $\tilde{q}$, where $\tilde{q}(\mathbf{x},t,a) = \lim_{da\to 0} q_a(\mathbf{x},t)$, is

$$\mu_n(t,\lambda,\phi,p) = \frac{1}{q}\int_0^\infty a^n \tilde{q}\, da. \tag{5}$$

Taking a material derivative of equation 5 and then integrating by parts the evolution equation of the n-th moment of the age distribution gives, written in a "specific form",

$$\left(\frac{\partial}{\partial t} + \nabla\cdot\mathbf{v}\right)\mu_n = n\mu_{n-1} - \frac{E}{q}\mu_n. \tag{6}$$

This equation recursively defines the evolution of the n-th moment in terms of the first $n-1$ moments, where by definition $\mu_0 = 1$. Alternatively, by using the conservation of mass equation for q, this equation can be written in a "density form",

$$\left(\frac{\partial}{\partial t} + \nabla\cdot\mathbf{v}\right)(q\mu_n) = nq\mu_{n-1} + S^- q\mu_n. \tag{7}$$

Equation 6 and 7 can be used to directly calculate the age of a given tracer in a GCM. One only needs to gather the sources or sinks at each time step to incorporate this tool into their model. We can track the moments of the WV age distribution in a GCM, and in turn, spatially resolve the mean WV age as well as any other moments of the distribution. In theory, either equation 6 or 7 could be applied in a GCM. In practice we find that equation 7 is easier to implement, since the last term in equation 6 can become numerically unstable in the case of evaporation into very dry air.

2.2 Implementation in the Isca model

To test our method, the moments tracers were implemented into the Isca modelling framework (Vallis et al., 2018). To simulate n WV age moments tracers, the moist model was modified. In this model, evaporation from the surface and immediate condensation interacts with the convective relaxation and radiation schemes to calculate moisture tendencies that drive the evolution equation for q. The negative moisture tendencies from the convection and condensation schemes were separately aggregated into a sink of WV diagnostic (S^-). With S^-, the left-hand side of equation 7 was implemented into its separate module. Explicitly, $q\mu_n$ is a passive tracer in the model and is outputted as a diagnostic. Later on, μ_n is recovered by dividing $q\mu_n$ by q. So, for a given time step, the convection, then large scale condensation schemes are called first. For each, the negative moisture tendencies are collected and added to S^-. Then, the radiation, diffusion and hydrology modules modify the moisture profile and add on to the moisture tendency. To calculate the $q\mu_n$ tendency, values of q and μ_{n-1} at the previous time step, and S^- at the current time step are inputs to the implementation of equation 7. The q and $q\mu_n$ tendencies are then fed into the dynamical core of the model, and evolve as normal passive tracers.

© Author(s) 2026. CC BY 4.0 License.

We chose a configuration with realistic continents and fixed SSTs, which showed good agreement with reanalysis data (Vallis et al., 2018). We used a T42 resolution, a time step of $dt = 720s$ and an hybrid pressure coordinate system composed of 45 levels, with an RRTM radiation scheme (Mlawer et al., 1997), grid scale condensation (Frierson, 2007), Full Betts-Miller (FBM) convection scheme (Betts, 1986; Frierson et al., 2006) and bucket hydrology (Manabe, 1969). We ran the model at T85 resolution to confirm that the results were not sensitive to resolution (not shown). We performed experiments at both a reference Atmospheric Model Intercomparaison Project (AMIP) climate and constant SST change experiments, where we added an anomaly to all SSTs globally. The model ran for 30 years with the configuration described above, and the results were averaged over the final 5 years to avoid any spinup. For completeness, we verified that the specific humidity budget is closed (not shown). From there, we also show how the age-mass budget from equation 7 is also closed (not shown).

2.3 Parameterization of water vapor age spectrum

As previously mentioned, to estimate the full water vapor age spectrum using the calculated moments we need to parameterize the probability distribution function in terms of the first n moments. Based on previous work, the distribution of WV age is expected to take a shape that can range between an exponential and a Gaussian distribution (Wang-Erlandsson et al., 2014; Tuinenburg and van der Ent, 2019). The Gamma distribution meets these criteria and has been used to characterize the distribution of WV age in Lagrangian experiments (Tuinenburg and van der Ent, 2016, 2019). The Gamma distribution is defined as

$$\mathcal{P}(a) = \frac{a^{(\alpha-1)}\exp(-a/\beta)}{\Gamma(\alpha)\beta^{\alpha}} \tag{8}$$

where Γ denotes the Gamma function. The parameters α and β can be calculated as,

$$\beta = \frac{\mu_2 - \mu_1^2}{\mu_1} \quad \text{and} \quad \alpha = \frac{\mu_1}{\beta}. \tag{9}$$

From parameters α and β, any moments of the distribution can be evaluated as the derivative of the moment generating function,

$$\mu_n = \frac{\partial^n}{\partial y^n}(1-\beta \cdot y)^{-\alpha}\Bigg|_{y=0}. \tag{10}$$

Using the Gamma distribution (equation 8) as a parametric approximation of the true WV age distribution, we can use the first two moment tracers (or equivalently the mean and shape parameter) to calculate the WV age distribution.

2.4 Age of precipitation

With our ability to track the WV age at every grid point and time step, it is possible to calculate the age of precipitation being produced, ν. We defined it as the mean age of the WV associated with the precipitation that reaches the surface. Our model (described in section 2.2) has both grid-scale condensation and sub-grid scale convection schemes, which change atmospheric

© Author(s) 2026. CC BY 4.0 License.

moisture. Importantly, our model makes a pseudo-adiabatic assumption, so that all condensed water is removed from the column at the end of the time step. A parcel at the i-th vertical level is subject to some change in q, dq_i, from both schemes. The total amount of condensed water vapor at level p_i can be found by summing from the top of the atmosphere:

$$dq_l(p_i) = \max\left(-\sum_{j=i}^{0} dq_j, 0\right). \tag{11}$$

If $dq_i < 0$, a quantity $|dq_i|$ of WV with mean age τ_i is condensed and added to the falling precipitation. The age of the precipitation accumulated at the i-th level is found by iteratively summing over the ages of the liquid water from the levels above:

$$\nu(p_i) = \frac{|dq_i|\tau_i + |dq_l(p_{i-1})| \cdot \nu(p_{i-1})}{dq_l(p_i)}. \tag{12}$$

If $dq_i > 0$, there is some evaporation, and it reduces the total water content. The age distribution has not changed between the $(i-1)$-th and i-th levels, but the amount of liquid water, and in turn its weight in the column mean of WV age, has reduced so that

$$\nu(p_i) = \nu(p_{i-1}) \quad \text{and} \quad dq_l(p_i) < dq_l(p_{i-1}). \tag{13}$$

Therefore, starting from the top layer, equation 11, 12 and 13 can be used to sum the mean age of precipitation at the surface. Although we have not calculated the higher moments of the precipitation age distribution, a similar method can be used to calculate the subsequent moments in future experiments.

3 Results

3.1 Control experiment

3.1.1 Climatology

The model moisture climatology and circulation are shown in figure 2. The majority of the WV is located around the equator, and its concentration drops off as you go poleward (figure 2A), similar to observations. Figure 2B shows the time and zonal average of the relative humidity, RH. The distribution of RH is also very similar to observations, with typical values near 80% throughout most of the troposphere, with the exception of the subtropical mid and upper troposphere, where RH has a minimum of about 25%. Above 200 hPa, RH drops below 15%. The moisture sink (S^-) is concentrated near the tropical surface, with extensions into the tropical and midlatitude mid-troposphere (figure 2C), indicating where WV is being removed from the atmosphere. The large maximum near the surface is due to the sub-grid scale convection scheme, which removes WV in the lower troposphere and adds thermal energy in the upper atmosphere (approximating the effects of convectional latent heating, Frierson, 2007), while the midlatitude and tropical midtropospheric maxima are from grid-scale condensation. The mean meridional circulation primarily moves WV through the tropical Hadley cell (figure 2D) (Trenberth and Stepaniak,

© Author(s) 2026. CC BY 4.0 License.

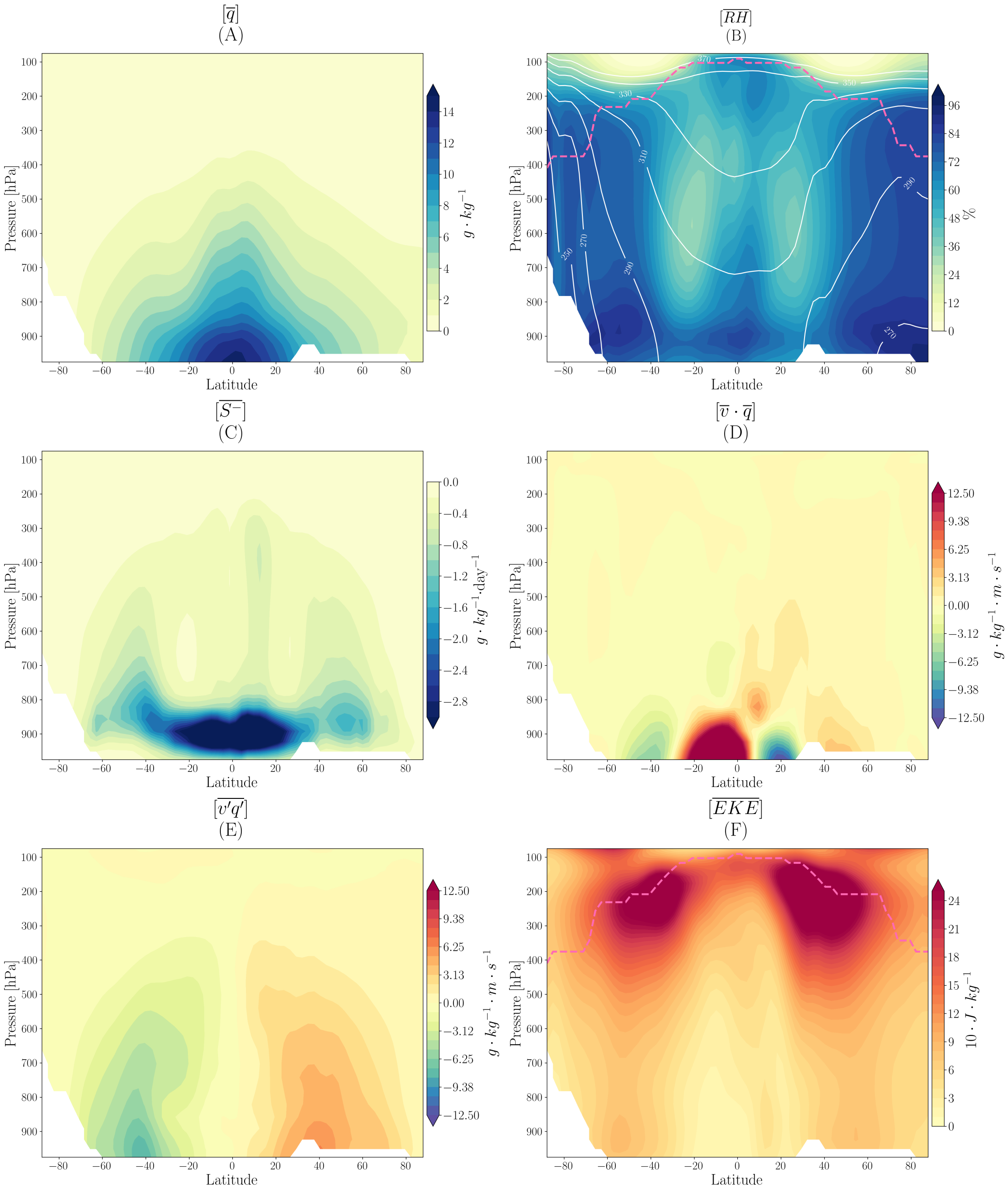

Figure 2. Time and zonal averages of (A) specific humidity, $[\overline{q}]$, (B) relative humidity, $[\overline{RH}]$, (C) the negative contribution of the moisture tendency from condensation and convection, $[\overline{S^{-}}]$, (D) the mean meridional moisture transport, $[\overline{v} \cdot \overline{q}]$, (E) the transient eddy meridional moisture transport, $[\overline{v'q'}]$, and (F) the eddy kinetic energy, $[\overline{EKE}] = [(\overline{u'^2} + \overline{v'^2})/2]$. The white contours indicate the isentropes, and the pink dashed line indicates the tropopause height, defined as the level where the atmospheric lapse rate drops below $2K \cdot km^{-1}$.

https://doi.org/10.5194/egusphere-2025-6395
Preprint. Discussion started: 23 January 2026
© Author(s) 2026. CC BY 4.0 License.

2003), and the eddies move WV through the midlatitude atmosphere ($\overline{v'q'}$, figure 2E) (Seager et al., 2010), consistent with the distribution of eddy kinetic energy: $\overline{EKE} = (\overline{u'^2} + \overline{v'^2})/2$, which is largest in the midlatitudes (figure 2F).

The regional patterns and mechanisms of vertical water vapor transport, evaporation, and precipitation generally match between the model and observations (figure 3), which we present for later comparison to our age results. Over the equator, there is a vertical moisture transport by the mean circulation (figure 3A and 3C), resulting in strong amounts of precipitation (figure 3E). Water vapor moves downwards in a number of important subsidence zones (figure 3A and 3C). This include the west coast of South America and South Africa, as well as Northeastern Africa (figure 3A). The eddy transport (figure 3B) dominates in two regions, one over the east coast of North America and the other over the Tibetan plateau and South-East Asia, reflecting the midlatitude storm tracks and the South Asian Monsoon. Evaporation (figure 3D) is strongest in the subtropical oceans, and precipitation (figure 3E) is largest in the ITCZ and midlatitude storm tracks.

3.1.2 Spatial distribution of the zonal mean water vapor age and shape Parameter

Figure 4A presents the time and zonal average of the mean WV age over the troposphere, calculated from the implementation of equation 7 for the first moment of the age distribution (μ_1) in the Isca model. The mean WV age is generally lower near the surface and increases with height. It reaches a tropospheric maximum near the tropopause (pink dashed line). Near the surface, the age is lower in the tropics and midlatitudes, and increases towards the poles. Over the equator, WV is the youngest near the surface (∼2.5 days) and increases with height to about 7.5 days in the mid-troposphere. Near the tropopause, the age decreases back to about 5-6 days. In the subtropics, poleward of this vertical minimum band, is a local maximum in age with values around 12-15 days, aligned with the isentropes ($\theta = 330K$). Over the midlatitudes, the surface minimum extends vertically from the surface to the mid-troposphere. Finally, in the troposphere, the age of WV is highest over the poles. The minimum in age over the midlatitude is greater, and extends higher in the Southern Hemisphere due to the higher mean WV age over Antarctica.

For the shape parameter, $s < 1$ is associated with more turbulent transport while, $s > 1$ indicates that a strong transport pathway dominates the overall transport (Waugh and Hall, 2002; Orbe et al., 2016). Figure 4B presents the time and zonally averaged shape parameter over the troposphere. Generally, $s < 1$ near the surface, $s > 1$ in the mid troposphere and again $s < 1$ aloft. It takes its lowest values near and above the tropopause. In the tropics, near the surface, $s \sim 1$ over the equator and decreases as you go poleward. Aloft, s increases to values over 1, with a local maximum around 700 hPa. Then, it drops back below 1 into a local minimum around 400 hPa. Over the midlatitudes, s is very close to 0. Between 700 and 300 hPa, $s > 1$ and drops back below 1 as you approach the tropopause. Over the poles, $s > 1$ from the surface to the tropopause. The maxima in s for both hemispheres are in the mid-troposphere, over the poles.

In the tropics, near the surface, evaporation introduces "young" water vapor that mixes into the atmosphere and the ITCZ updraft removes WV from the tropics, as was evident by the value of S^- (figure 2C). This reduces the mean WV age in that

https://doi.org/10.5194/egusphere-2025-6395
Preprint. Discussion started: 23 January 2026
© Author(s) 2026. CC BY 4.0 License.

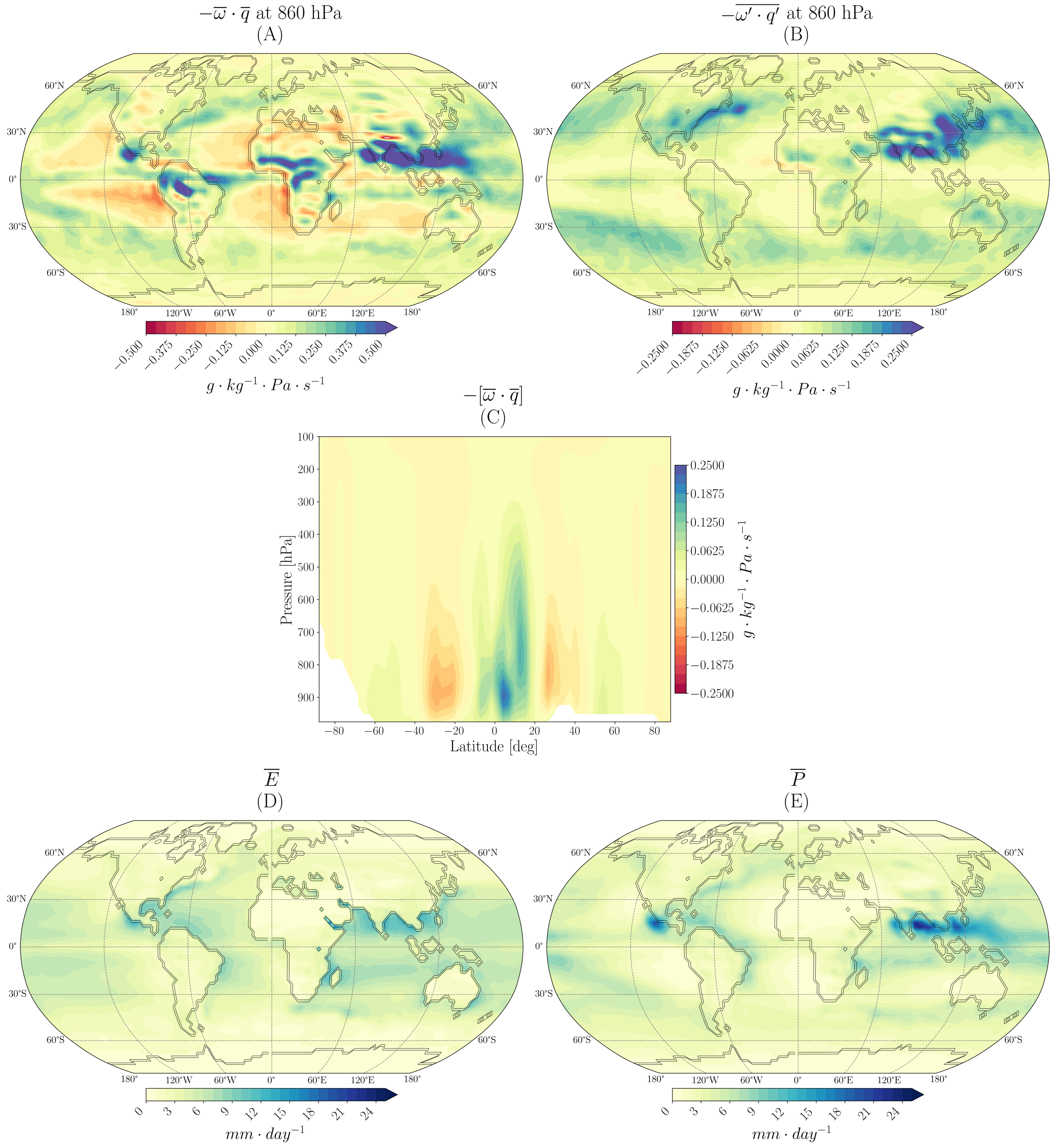

Figure 3. Time average of the (A) negative vertical moisture transport on a 860 hPa surface, $-\overline{\omega}\cdot\overline{q}$, (B) negative vertical transient eddy moisture transport on a 860 hPa surface, $-\overline{\omega'\cdot q'}$, (C) zonal average of negative vertical moisture transport $-[\overline{\omega}\cdot\overline{q}]$, (D) evaporation, E, and (E) precipitation rate, P. Positive values indicate vertical transport.

https://doi.org/10.5194/egusphere-2025-6395
Preprint. Discussion started: 23 January 2026
© Author(s) 2026. CC BY 4.0 License.

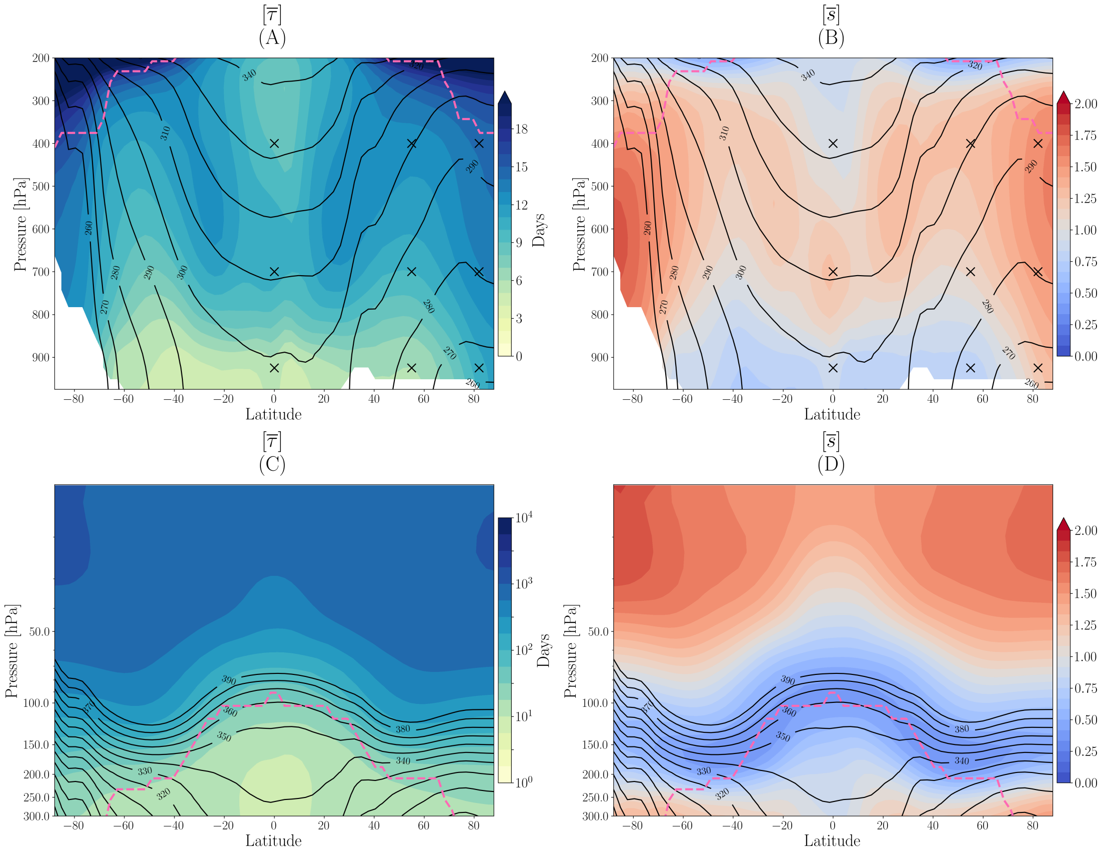

Figure 4. Time and zonal average of (A, C) the mean water vapor age, $[\overline{\tau}]$, and (B, D) the shape parameter, $[\overline{s}]$, in (A, B) the troposphere and (C, D) the stratosphere. The stratospheric mean age colorbar (C) is on a log scale. Black contours highlight the isentropes. The pink dashed line indicates the tropopause height. The black crosses indicate the points where samples of the local distribution of WV age were calculated and presented in figure 5.

region (figure 4A). Furthermore, the moisture convergence gathers water from the subtropics, which took different transport pathways to arrive, so s is also low . Then, the WV is transported vertically by the updraft. This injects "younger" WV into the high troposphere (figure 4A). Around 700 hPa, there is only one main type of transport taking WV to this height, the updraft of the ITCZ. This is shown by the local maximum in s. Over the midlatitudes, the transient eddies mix newly evaporated WV with "older" WV aloft. This is evident by the minimum in WV age extending from the surface to the mid-troposphere and the low values of the shape parameter in the region. On the other hand, the majority of the WV in the region between 700 and 400 hPa gets there via the descending branches of the Hadley cell, which results in greater values of s. In the poles, the WV is generally older because there is less surface evaporation (figure 3C) and the circulation is weaker. The isentropic mass transport driven by midlatitude eddies takes WV from the midlatitude to the poles (Fajber et al., 2018). The high shape parameter values over the poles indicate that this transport dominates in the region. By investigating transit time distribution from the Northern

© Author(s) 2026. CC BY 4.0 License.

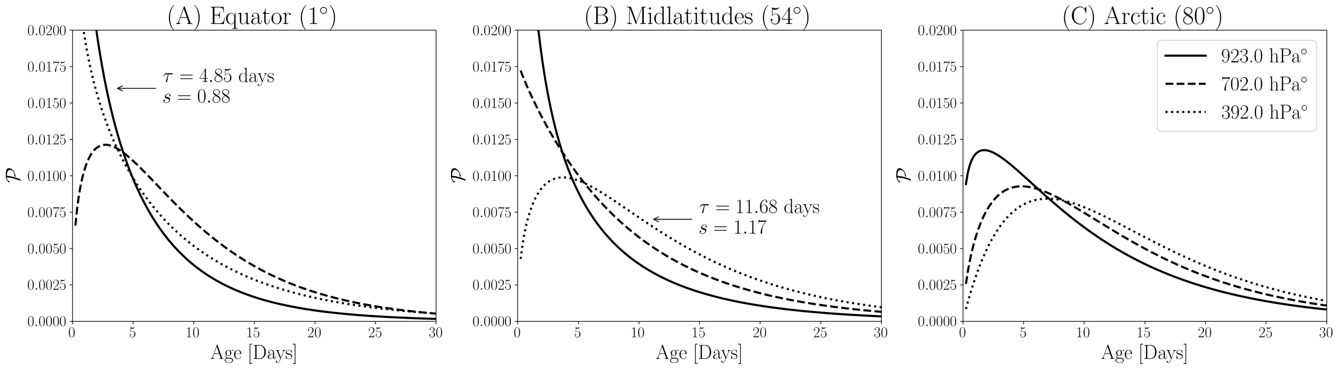

Figure 5. Sample gamma distributions of the local WV age distribution from the first 2 moments tracers at the points denoted on figure 4. Locations with the same latitude but different pressure levels are presented on each panel. Namely, (A) : 0°, (B) : 54° and (C): 80°. All distributions were obtained via equations 8, 9 and the first 2 moments of the WV age distribution. The Gamma distributions were evaluated on $t \in]0, 30 \text{ days}]$.

Hemisphere midlatitude surface, Orbe et al. (2016) found similar distributions that were consistent with the isentropic transport from the midlatitude to the poles.

For a moment, we will shift our focus to the upper troposphere, lower stratosphere (UTLS) region (between 300 and 50 hPa) and beyond. In this region, the low moisture content is evident from the very low values of q and RH (figures 2A and 2B). Because of the low moisture content of the stratosphere, the air is rarely saturated, and there are no sinks of WV (figure 2C). This results in high values of the mean WV age over the UTLS region (figure 4C). On figure 4C, the mean WV age increases from 20 to over 100 days as you cross the tropopause. It then increases to nearly 1000 days in the upper parts of the stratosphere (although we note that the age is less than the runtime of the model, indicating the stratosphere water vapor has equilibrated). According to re-analysis, most of the exchange between the stratosphere and troposphere is done over the midlatitudes via the tropopause gap (Langille et al., 2020). WV from the lowermost stratosphere (portion of the stratosphere where $310K < \theta < 380K$) travels along the isentropes to the upper troposphere and vice versa (Holton et al., 1995). This is visible in the intrusion of dry air from the stratosphere to the underworld by the minimum in RH near the tropopause on figure 2B (along $\theta = 330K$) and the EKE maxima in the tropopause over the midlatitudes from figure 2F. This is also reflected in the mean WV age and shape parameter on figure 4, not only is there a local maximum in WV age in the mid to high tropopause, poleward of the updraft's minimum (along $\theta = 330K$) but $s < 1$. The air is this region is descending isentropically and drying, producing relatively low relative humidity (c.f. Figure 2B) and high water vapor age (Galewsky et al., 2005). After entering the stratosphere over the tropics, the Brewer-Dosbon circulation (BDC) the air mass rises, then advances poleward, only to then diabatically descend in the lowermost stratosphere, and later on into the troposphere, over mid to high latitudes (Dessler et al., 1995). The mean WV age and shape parameter both increasing as you go up and polewards reflects the WV transport at these heights. For example, the upper stratosphere is primarily ventilated by the BDC, so it has a relatively high values of s.

© Author(s) 2026. CC BY 4.0 License.

On figures 4A and 4B, 9 locations were marked by a cross. Figure 5 presents the local Gamma distribution of these points. The first 2 moments were used to parametrize the distributions via equation 8 and 9. Panels A, B, and C compare locations with the same latitude ($0°$, $54°$ and $80°$), but different pressure levels. Over the equator, age increases with height (figure 4A). At 921 hPa, the distribution has a mean of 4.85 days and a shape parameter of 0.88. There is a clear difference between the exponential-like distribution near the surface and the top of the updraft (solid and dotted curves), and the Gaussian-like distribution within the strongest region of the updraft (dashed curve). In the updraft region, the WV aged collectively, and so as the mean age increased, the standard deviation did not change much, and the resulting distribution is closer to a Gaussian. In the midlatitudes (figure 5B), the distributions shift from "young" water evaporated near the surface to water that has been mixed by the midlatitude eddies aloft. At 396 hPa, the distribution has a mean of 11.68 days and a shape parameter of 1.17. This region is dominated by fewer transport pathways (descending branch of the Hadley cell), so the mean is greater aloft and the WV ages are more normally distributed. Finally, if we compare points at the equator (figure 5A) at 700 hPa and the poles (figure 5C), both are in a region of high shape parameter, and have a similar distribution. Even though both are very different transport pathways, the isentropic transport of WV from the midlatitudes to the poles and the ITCZ updraft yield similar WV age distributions.

3.1.3 Regional patterns of the mean water vapor age and shape Parameter

Figure 6A presents the time average of the mean WV age on a 860 hPa surface. Generally, the age is greater in the poles and increases towards the mid to low latitudes. In the tropics, over the oceans, the mean WV age peaks over the equator and decreases poleward. Over the land, this peak is not present. Maxima are located on the west coast of South America and South Africa, over the Eastern Pacific and over North Africa. The WV age is minimal in the location of the North American and South Asian monsoon, as well as inland South America and Southwestern Africa. In the midlatitudes, there are local maxima over the Tibetan plateau and on the west coast of North Africa and North America. By contrast, the mean WV age is minimized on the east coast of North America and over the South Pacific. Figure 6B presents the time average of the shape parameter on the same 860 hPa surface. Generally, $s > 1$ in the poles and drops below 1 equatorward of the poles. In the tropics, there are some regions where $s > 1$, namely, the equator line, the west coast of the Americas and Africa, and over North Africa. Over most of the mid to low latitudes, WV can travel freely in the planetary boundary layer (PBL), so the subsequent turbulent transport is reflected by $s < 1$. Over the poles, as we saw earlier, it takes a greater amount of time for WV to get there as it moves along isentropic lines, and $s > 1$.

Over the equator, there is a strong vertical uplift of WV (figures 3A and 3B). The WV that converges, rise, does not condense, and makes it to 860 hPa, has a mean age greater than its immediate poleward neighbour, and its shape parameter is over 1 due to the dominant transport of the updraft and convergence zone (figures 6A and 6B). On the west coast of the Americas and Africa, there are subsidence regions, which explains the associated maxima in s. Higher precipitation and evaporation regions (figures 3C and 3D) also reduced the mean WV age over the location of the North American and South Asian monsoon, as well

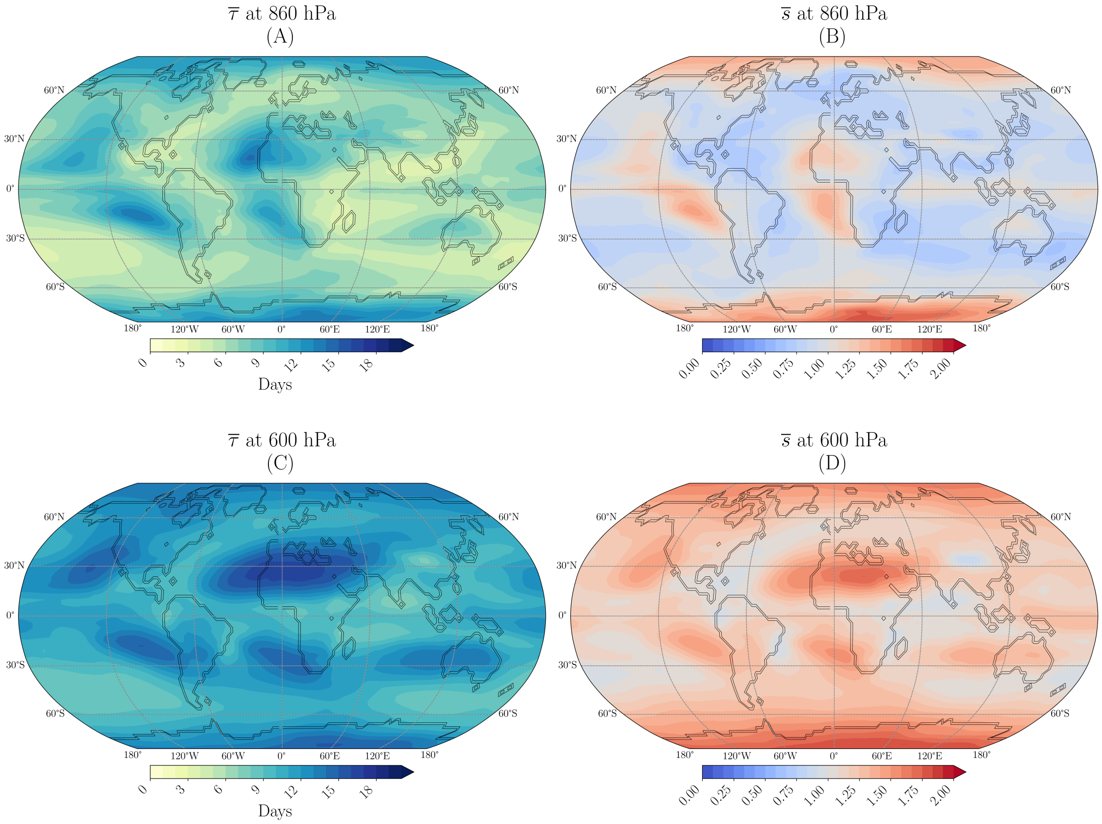

Figure 6. Time average of (A, C) the mean water vapor age, $\overline{\tau}$, and (B, D) shape parameter, $\overline{s}$ at (A, B) 860 hPa and (C, D) 600 hPa.

as inland South America, Southwestern Africa and North Africa. In the midlatitudes, the reductive impact of the North Atlantic and North Pacific storm tracks are clear on the distribution of WV age. At the start of the storm tracks (Western Atlantic and Pacific), the high precipitation reduces the mean WV age, and the mixing by the eddies takes the shape parameter closer to 0. At the end of the storm tracks (North eastern Atlantic and Pacific), the age is greater since the WV that reached this location along the storm track has travelled a good distance. Furthermore, the distribution will have a greater shape parameter than the region due to the storm tracks being a more dominant transport pathway for WV (Orbe et al., 2016).

Figure 6C presents the time average of the mean WV age on the 600 hPa surface. As in figure 4, the WV age is higher at 600 hPa than at 860 hPa. The mean WV age is generally lower over the equator, increases to a local maximum around the subtropics, decreases in the midlatitudes and increases again in the poles. In the subtropics, there is a zonally alternating pattern of highs and lows. Maxima are located on the west coast of the Americas and South Africa, over North Africa, and in the Indian Ocean. Minima are placed over the location of the North American and South Asian monsoon, the middle of the Pacific Ocean and the west coast of South America. In the midlatitudes, notable minima in WV age are located across the Southern Ocean and over the North Atlantic. In those regions, midlatitude eddies create vertical moisture transport (figure 3A and 3B), bringing "young" WV from the lower levels, reducing the mean WV age at 600 hPa.

Figure 6D presents the time average of the shape parameter on a 600 hPa surface. At this level, values of s are generally larger than on the 860 hPa surface due to the longer time scales required for WV to reach the 600 hPa level. It peaks in regions like the west coast of the Americas and South Africa, over North Africa, and in the Indian Ocean. It is also greater than 1 around the equator. There are some regions where $s < 1$. These regions include the west coast of South America, the Northeastern Atlantic, the location of the South Asian monsoon, and the Southern Ocean from 60°E to 120°W. The strong maxima in WV age are associated with the previously mentioned subsidence zones of the 860 hPa surface. Here, the WV had to travel through the circulation cells, which means it would be older than in nearby regions. Unlike 860 hPa where generally $s < 1$, at 600 hPa $s > 1$, which demonstrates that most of the water vapor is reaching this level through defined transport pathways, as opposed to the more chaotic transport pathways of the lower atmosphere. However like the 860 hPa surface, we can still see the effect of the high precipitation regions, midlatitude transient eddies, and the storm tracks on s. Over the Southern Ocean, the effect of the transient eddies is very clear in the minimum in WV age and s.

Figure 7A shows a map of the time average of the mean age of precipitation calculated using equation 11, 12 and 13. It is defined as the mean age of the precipitated WV reaching the surface (see section 2.4) and weighted by precipitation amounts per time step. The age of precipitation peaks in the poles (above 10 days) and is lower (2-7 days) in the mid to low latitudes. In the tropics and midlatitudes, some of the maxima and minima are generally aligned with the pattern from figure 6A, but with higher maxima.

We compare the age of precipitation to the time average of the moisture-weighted vertically averaged WV age, defined as

$$\frac{\overline{\{\Lambda\}}}{\overline{W}} = \frac{\overline{\{q\tau\}}}{\overline{\{q\}}}, \tag{14}$$

where $\Lambda = q\tau$ (figure 7B). The mean age of precipitation can differ from the WV age based on the vertical distribution of condensation. The vertically average WV age is generally high in the poles and decreases in the mid to low latitudes. Over the equator, the WV age peaks and drops off in the tropics. In the tropics and midlatitudes, most of the maxima and minima are aligned with the pattern from figure 6A, but with generally higher values. Notable different maxima are located over the Tibetan plateau, the Rocky Mountains and Eastern Antarctica. These high topography regions exhibits higher values of $\frac{\overline{\{\Lambda\}}}{\overline{W}}$ due to both the higher τ and the reduced number of vertical points.

Figure 7C presents the relative difference between $\overline{\nu}$ and $\frac{\overline{\{\Lambda\}}}{\overline{W}}$, defined as

$$R = \frac{\frac{\overline{\{\Lambda\}}}{\overline{W}} - \overline{\nu}}{\frac{\overline{\{\Lambda\}}}{\overline{W}}}. \tag{15}$$

https://doi.org/10.5194/egusphere-2025-6395
Preprint. Discussion started: 23 January 2026
© Author(s) 2026. CC BY 4.0 License.

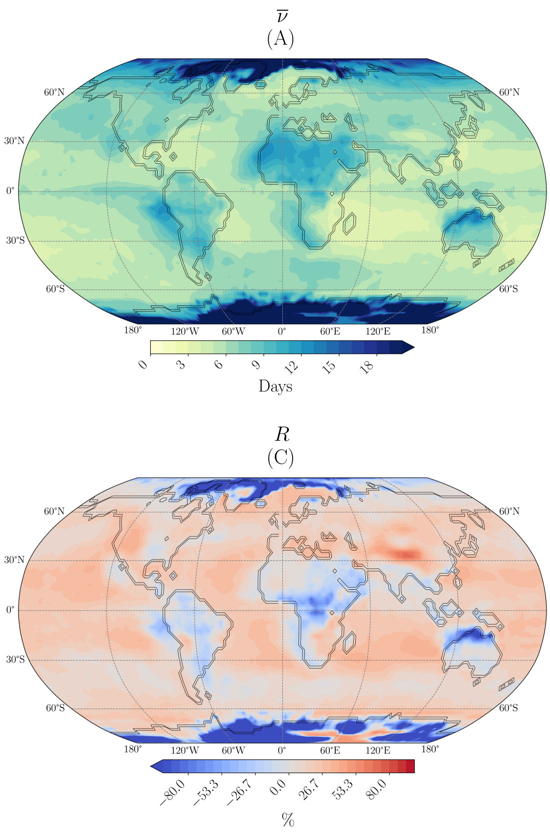

Figure 7. Time average of (A) the mean age of precipitation, $\overline{\nu}$, (B) the vertical moisture weighted average of the mean WV age, $\overline{\frac{\{\Lambda\}}{W}}$, and (C) the difference between $\overline{\frac{\{\Lambda\}}{W}}$ and $\overline{\nu}$, R.

Positive values of R indicate that the mean WV age in the column is greater than the age of precipitation. The difference is positive over most of the oceans, with slight maxima over some high topography regions like the Tibetan plateau, the Rocky Mountains and Eastern Antarctica. As it is clear from figures 6A and 6C, the mean WV age is high in a column over a subsidence zone located over the ocean, since WV has had to travel greater distances to reach these points. But, in these regions, the precipitation comes from shallow convection. When we look at the sinks of WV over the same latitudes (figure 2C), we can see how the sinks of WV are concentrated below 800 hPa. Therefore, the WV that rains out is typically from lower levels and, in turn, is much younger. So, in general, regions in red, where $R > 0$, can be associated with precipitation that comes from lower levels or is from local sources, while, regions in blue, where $R < 0$, can be associated with precipitation coming from higher up in the column, or from more remote sources. For example, R is maximum over the Tibetan plateau, the Rocky Mountains, and Eastern Antarctica, regions of high topography and low in precipitation (figure 3D). In this case, $R > 0$could indicate that most of the precipitation is from local sources. In the North American and South Asian monsoon region, where there is high vertical transport and precipitation (figures 3A and 3D), $R < 0$, indicating that WV is precipitating

https://doi.org/10.5194/egusphere-2025-6395
Preprint. Discussion started: 23 January 2026
© Author(s) 2026. CC BY 4.0 License.

high up in the column. In the poles, precipitation mainly comes from remote sources of WV due to the cold temperature and low relative humidity, which is reflected by $R < 0$ in this region.

3.2 Climate change experiment

3.2.1 Scaling of global water vapor age with temperature

With our age moments tracer, we can calculate the globally averaged mean precipitation age, $\langle \nu \rangle$, as well as the vertical, moisture-weighted, globally averaged mean WV age, $\frac{\langle \{\Lambda\} \rangle}{\langle W \rangle}$. We compare them with TUT ($\frac{\langle W \rangle}{\langle P \rangle}$) and investigate how they scale with temperature (figure 8). When the global average is performed over entire atmosphere (figure 8A), $\frac{\langle W \rangle}{\langle P \rangle}$ and $\frac{\langle \{\Lambda\} \rangle}{\langle W \rangle}$ match almost exactly, and their scaling rates, 4.82% K^{-1} and 4.93% K^{-1}, differ only by 0.11 % K^{-1}. Although $\langle \nu \rangle$ stays close to $\frac{\langle W \rangle}{\langle P \rangle}$ and $\frac{\langle \{\Lambda\} \rangle}{\langle W \rangle}$ (less than 1 day difference), it scales at a different rate of 3.16% K^{-1}. This shows how we can expect global TUT to be equal to a global average of the mean WV age, and, about equal to the global mean of precipitation age. But, the latter would evolve differently with climate change (although they match the wide range of anticipated scaling rates of 3-6% K^{-1}, Gimeno et al., 2021). On the other hand, when the averaged domain is constrained to the tropics (between 30°S and 30°N), $\frac{\langle W \rangle}{\langle P \rangle}$, $\frac{\langle \{\Lambda\} \rangle}{\langle W \rangle}$ and $\langle \nu \rangle$'s scaling rates increase to 5.33% K^{-1}, 5.52% K^{-1} and 3.62% K^{-1} (figure 8B). Additionally, $\frac{\langle W \rangle}{\langle P \rangle}$ is now consistently greater than $\frac{\langle \{\Lambda\} \rangle}{\langle W \rangle}$ by about a day. TUT has increased since, by considering the tropics, $\langle P \rangle$ reduced due to the omission of the midlatitude precipitation while $\langle W \rangle$ stayed about constant, as it is mostly concentrated in the tropics. The mean precipitation age and mean WV age decreased because, as we can see on figure 7B, the larger values of mean WV age and precipitation age are located outside of the tropics. Broadly, figure 8B shows how our previous assumption about the equivalence of $\frac{\langle W \rangle}{\langle P \rangle}$, $\frac{\langle \{\Lambda\} \rangle}{\langle W \rangle}$ and $\langle \nu \rangle$ breaks down over the tropics.

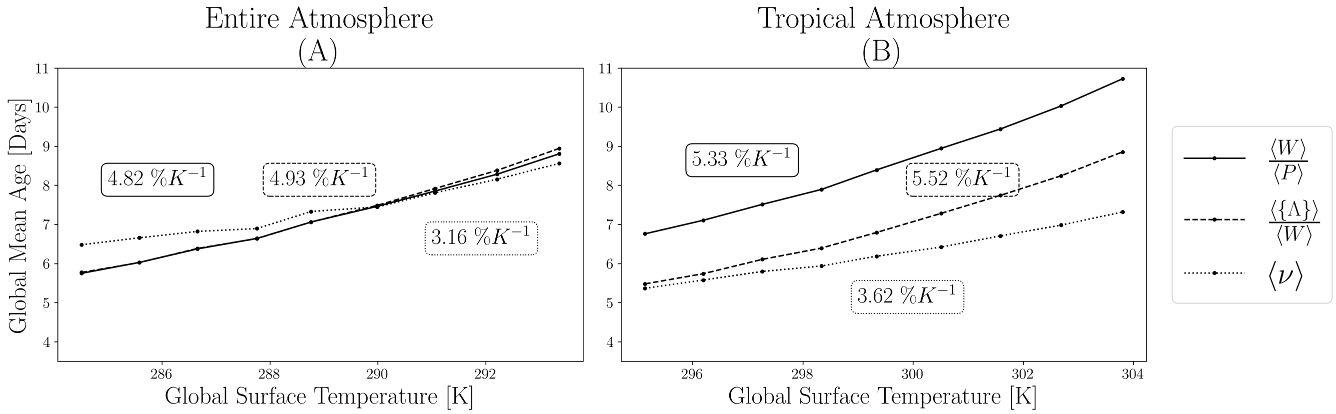

Figure 8. Turnover Time (TUT), $\frac{\langle W \rangle}{\langle P \rangle}$, the globally averaged moisture weighted mean WV age tracer $\langle q\tau \rangle / \langle W \rangle$, and the globally average precipitation age $\langle \nu \rangle$ as a function of globally averaged 2m air temperature. The averages were performed on (A) the entire atmosphere and (B) restricted to the tropics. The mean fractional increase rate between temperatures is marked on each panel for each quantities.

3.2.2 Climatology

To assess the changes in the mean WV age and shape parameter, and to compare with later figures, the anomaly per degree of warming of the quantities presented in figure 2 and 3 are presented in figure 9 and 10. They are calculated using the +2K climate experiment mentioned in section 2.2. Figure 10D and 9A show how increased evaporation over the oceans, leads to a rise in q throughout the atmosphere. Over the mid to low troposphere, $\Delta[\overline{q}]$ is about 7%, which is consistent with the Clausius-Clapeyron equation. With climate change, the ITCZ updraft is expected to strengthen (Byrne et al., 2018). It is indicated by the increased moisture convergence in the tropics on figure 9D and 10C. This causes the upper-level specific humidity to increase (figure 9A), RH to increase in the middle troposphere (figure 9B), and increases precipitation over the tropics (figure 10D). Furthermore, the minimum RH region in the middle troposphere shifts poleward (figure 9B) and, the sinks of WV increase in the sub-tropics over 800 hPa (figure 9C), indicating the poleward expansion of the Hadley cell (Frierson et al., 2007). The increased isentropic transport by the eddies and poleward shift of the isentropes (Wu and Pauluis, 2013) is evident by the change in the poleward and vertical transient eddy transport of WV (figure 9E and10B). Additionally, the eddy kinetic energy reduces in the mid to low troposphere due to the added moisture (Lutsko et al., 2024) (figure 9F). Finally, the tropopause rise increased EKE above the previous tropopause height (dashed blue line, figure 9F). Over the stratosphere, the exchanges between the troposphere and the lowermost stratosphere increase (Holzer and Boer, 2001), and this is shown by the maximum in $\Delta[\overline{q}]$ and $\Delta[\overline{RH}]$ near the tropopause (figure 9A and 9B). Overall, figure 9 and 10 shows that, in the tropics, we should expect a stronger updraft driven by a larger moisture convergence and a poleward expansion of the Hadley cell. In the midlatitudes, the eddies should become more intense and shift poleward. This will increase the moisture transport along the isentropes from the midlatitudes to the poles. Lastly, the exchanges between the stratosphere and troposphere also increase, suggesting a stronger BDC.

3.2.3 Spatial distribution of the mean water vapor age and shape parameter

We now look into the relative anomaly of the WV age distribution per degree of warming. Figure 11A presents the relative anomaly of the mean WV age with the +2K experiment. Generally, the mean WV age increased in the troposphere and decreased above the tropopause. The relative anomaly peaks in the tropics and reduces poleward. Figure 11B presents the zonally averaged relative anomaly of s with the +2K experiment. The change in shape parameter is maximum around the tropopause. Otherwise, over the tropics, near the surface, s decreased slightly, but increased above 900 hPa. Over the midlatitudes and the poles, it generally decreases and $\Delta[\overline{s}]$ reaches a minimum from 600 to 400 hPa. In the troposphere, because of the changes in the moisture transport with climate change we saw in section 3.2.2, WV will travel greater distances on average and, in turn, have a higher mean WV age. In the tropics, we saw that there was a stronger updraft, driven by a larger moisture convergence (figure 9). The stronger updraft increased s above 800 hPa, since this transport pathway is now more dominant. The larger moisture convergence reduced s below 800 hPa (figure 11B). WV from more varied array of locations now convergences to the ITCZ, which increases the standard deviation of the distribution. In the midlatitudes, the eddies and storm tracks become more intense and increase the isentropic transport (Wu and Pauluis, 2013). This increases the mixing in the mid-troposphere;

https://doi.org/10.5194/egusphere-2025-6395
Preprint. Discussion started: 23 January 2026
© Author(s) 2026. CC BY 4.0 License.

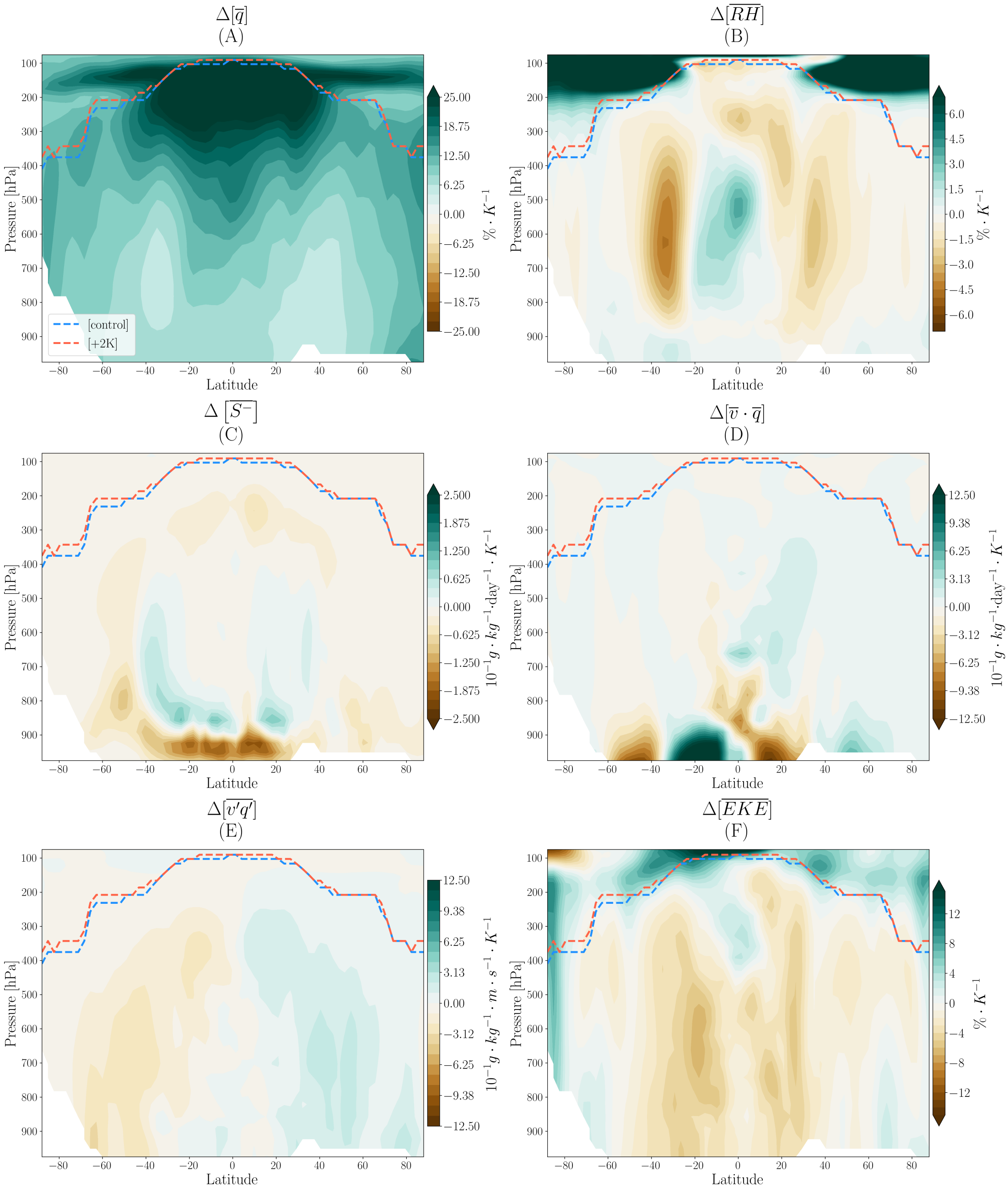

Figure 9. Time and zonally average of the +2K anomaly per K of (A) specific humidity, $\Delta[\overline{q}]$, (B) relative humidity, $\Delta[\overline{RH}]$, (C) the negative contribution of the moisture tendency from condensation and convection, $\Delta[\overline{S^{-}}]$, (D) the meridional moisture transport, $\Delta[\overline{v}\cdot\overline{q}]$, (E) the transient eddy meridional moisture transport, $\Delta[\overline{v'q'}]$, and (F) the eddy kinetic energy, $\Delta[\overline{EKE}]$. Primed quantities denote their deviation from their respective time average. The blue and red dashed line indicates the tropopause for the control and $+2K$ experiments, respectively.

https://doi.org/10.5194/egusphere-2025-6395
Preprint. Discussion started: 23 January 2026
© Author(s) 2026. CC BY 4.0 License.

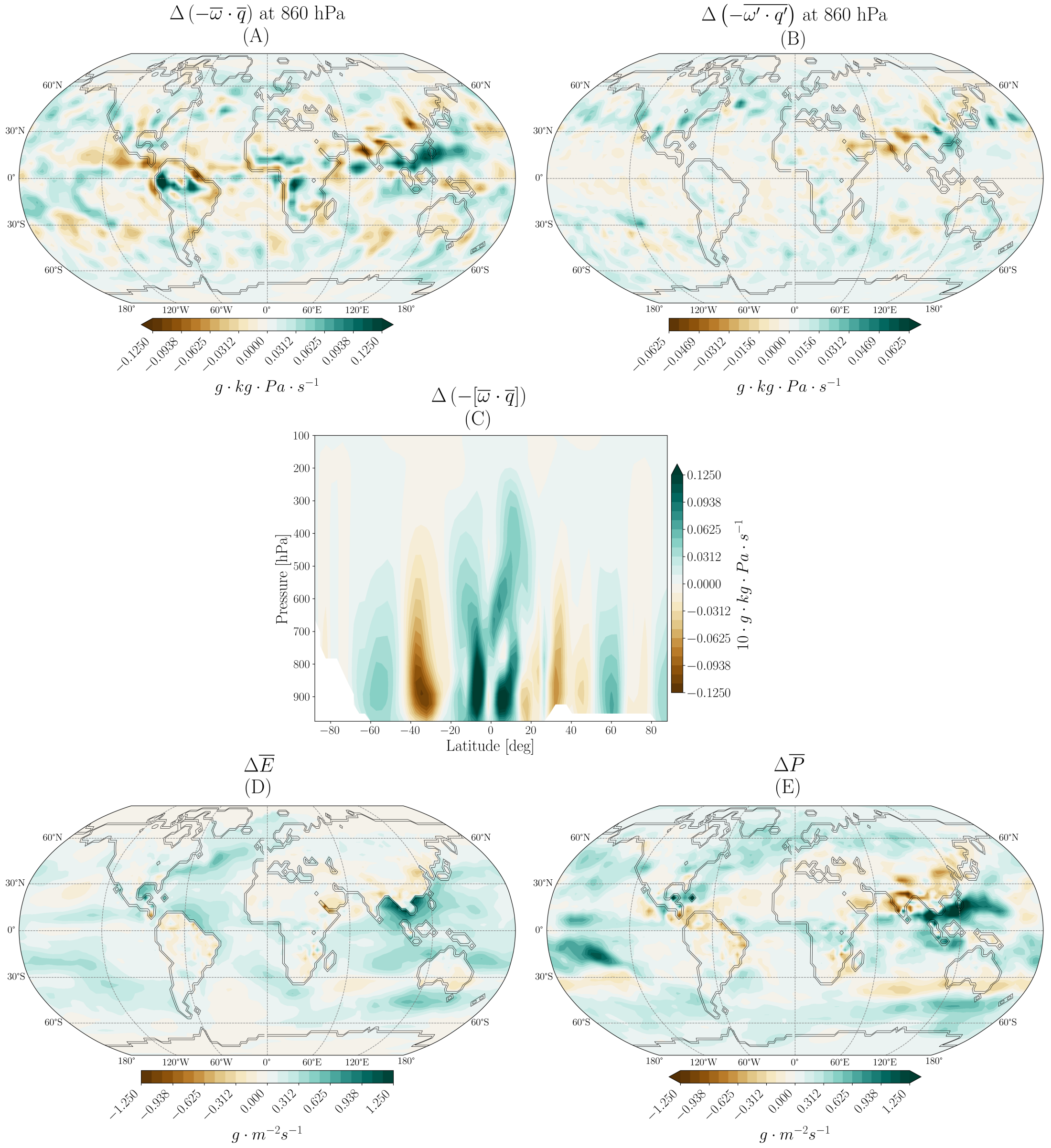

Figure 10. Time average of the anomaly with the +2K experiment of the (A) negative vertical moisture transport, $\Delta\left(-\overline{\varpi}\cdot\overline{q}\right)$, (B) negative vertical transient eddy moisture transport, $\Delta\left(-\overline{\omega'\cdot q'}\right)$, (C) zonal average of negative vertical moisture transport $\Delta\left(-[\overline{\varpi}\cdot\overline{q}]\right)$, (D) evaporation, ΔE, and (E) precipitation rate, ΔP. On figures 10A and 10B, the transport was calculated on a 860 hPa surface, and positive values indicate vertical transport.

© Author(s) 2026. CC BY 4.0 License.

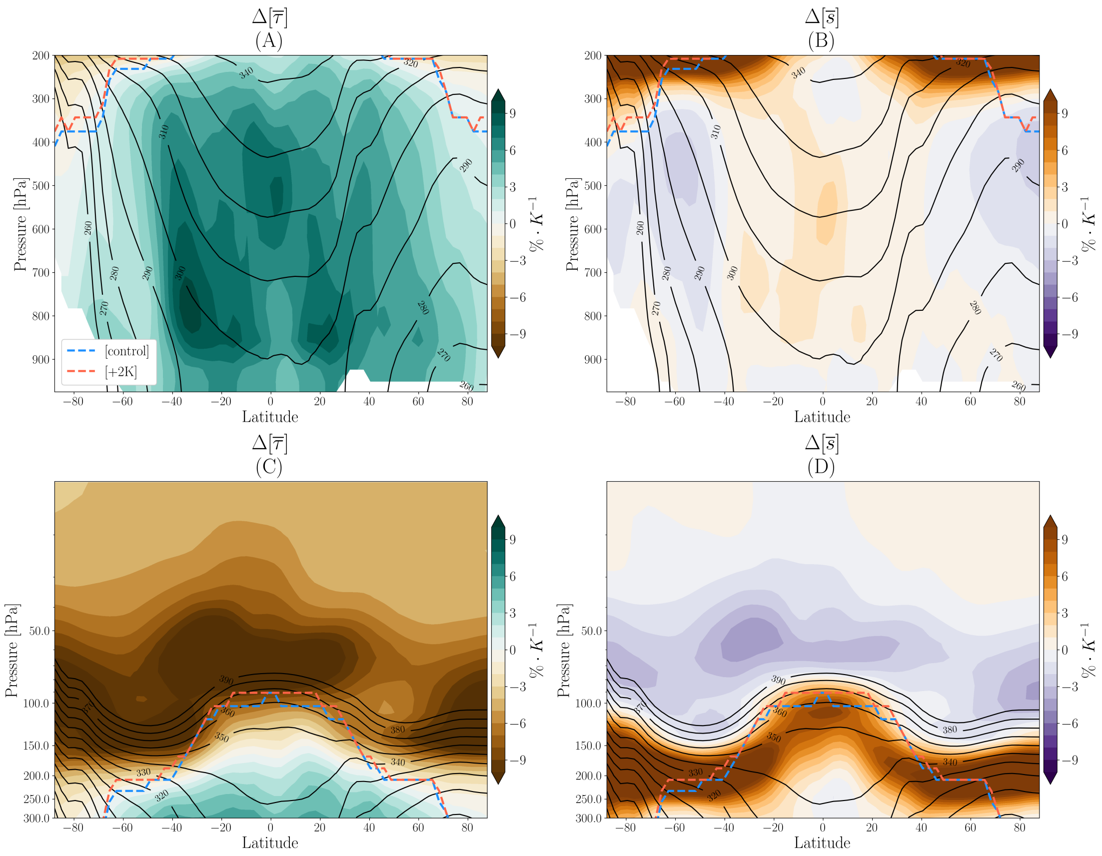

Figure 11. Time and zonal average of the relative anomaly with the +2K experiment for (A, C) the mean water vapor age, $\Delta[\overline{\tau}]$, and (B, D) the shape parameter, $\Delta[\overline{s}]$, in (A, B) the troposphere and (C, D) the stratosphere. Black contours highlight the isentropes. The pink dashed line indicates the tropopause height.

therefore, s decreased. The increased mixing works to reduce s by combining WV with more varied ages. Furthermore, the pattern of the change in s supports the widening of the Hadley cell and the poleward shift of the midlatitude eddies.

Turning to the stratosphere, figure 11C presents the zonally averaged relative anomaly of the mean WV age with the +2K experiment over the UTLS region. Above the tropopause, the mean WV age decreased. Over the tropics, $\Delta[\overline{\tau}]$ is maximum right above the tropopause. Over the midlatitude and the poles, $\Delta[\overline{\tau}]$ peaks below 100 hPa and is aligned with the isentropes. Along the tropopause, the increase in s (figure 11D) is large. Immediately above the tropopause s decreases slightly, while above this layer, it increases weakly. The increased BDC ventilates the stratosphere more effectively bringing younger WV into the region, which reduces the mean WV age (figure 11C). Additionally, the exchanges over the tropics and through the tropopause gap increased (figure 9), and the enhanced mixing leads to further decreases in s in the extratropical stratosphere. In the corners of the stratosphere, the stronger circulation can now bring WV there more effectively. Therefore, the transport pathway is more dominant in this region, and s increased near the top of the atmosphere (figure 11D). Finally, along the tropopause, s increased significantly. This indicates a vertical shift in the region of transition from $s > 1$ and $s < 1$ (figures 4B and 4D), which is consistent with the decreased strength of the Hadley cell and the increased tropopause height (Vallis et al., 2015).

3.2.4 Regional patterns of the mean water vapor age and shape Parameter

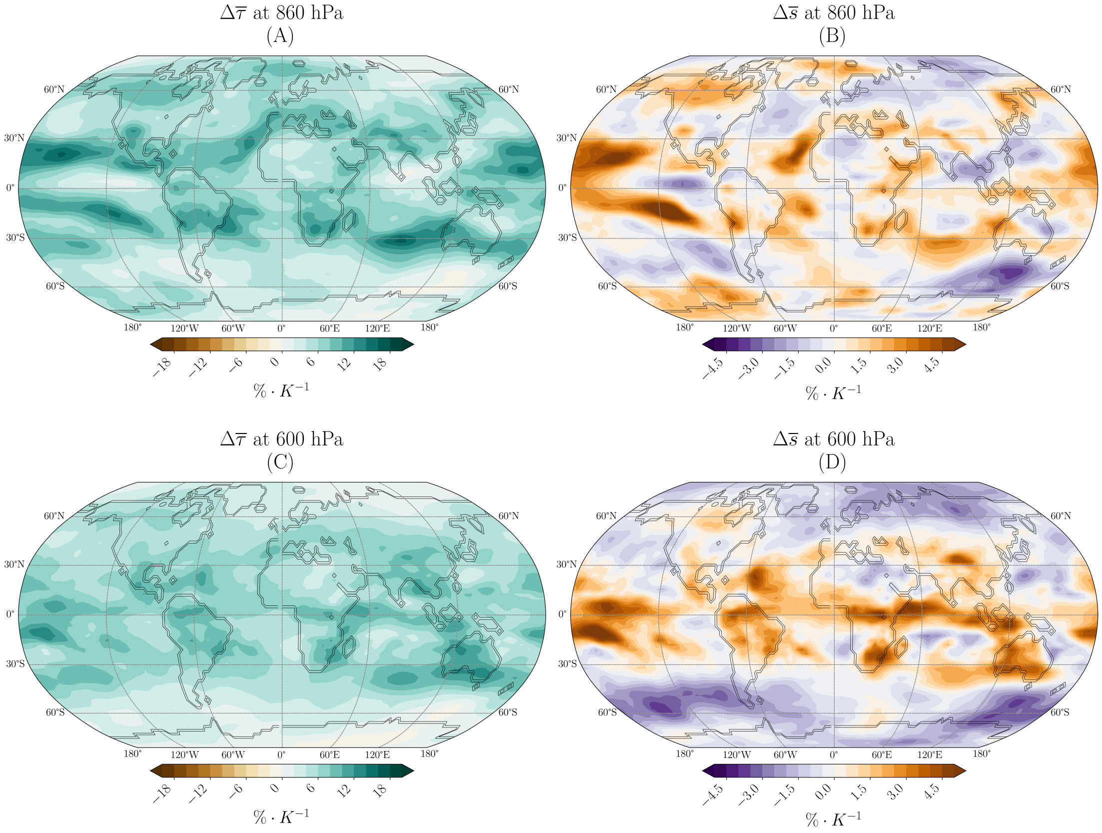
$\Delta\overline{\tau}$ at 860 hPa (A)

$\Delta\overline{s}$ at 860 hPa (B)

$\Delta\overline{\tau}$ at 600 hPa (C)

$\Delta\overline{s}$ at 600 hPa (D)

Figure 12. Time average of the anomaly of the +2K experiment for (A, C) the mean water vapor age, $\Delta\overline{\tau}$, and (B, D) shape parameter, $\Delta\overline{s}$ at (A, B) 860 hPa and (C, D) 600 hPa.

Figures 12A and 12B present the relative anomaly of the mean WV age and the shape parameter on a 860 hPa surface. Generally, τ increased over the entire globe. But, in the midlatitudes, there are regions where there are little to no changes, like the North Atlantic, Northeast Pacific, the Southern tip of South America and the location of the South Asian monsoon (figure 12A). The intensification of the storm tracks and midlatitude eddies acted to slow down the general increase in mean WV age (figure 12A), and the increased mixing reduced s (figure 12B) in those regions. At 600 hPa (figures 12C and 12D), τ increased almost everywhere, s increased over the tropics, reflecting the increased strength of the ITCZ updraft, and decreased over the midlatitudes, signature of the intensified eddies.

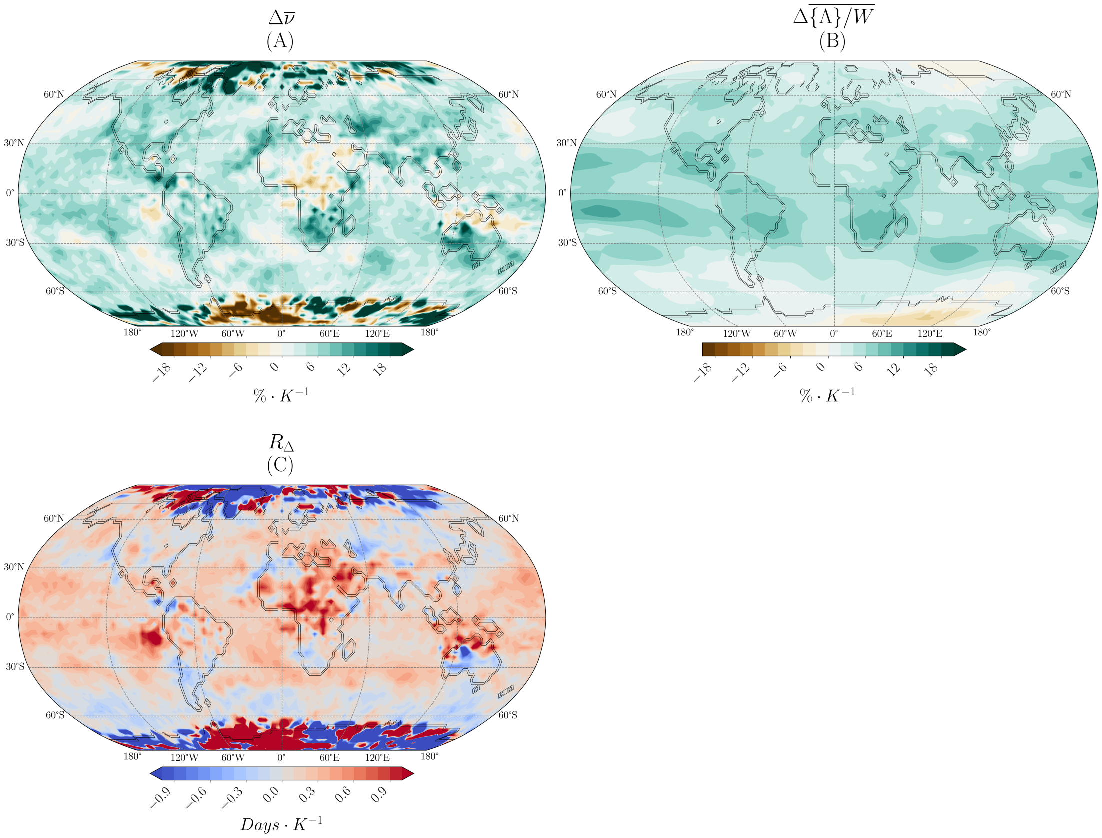

Figure 13. Relative anomaly of the time average of (A) the mean age of precipitation, $\Delta\overline{\nu}$, (B) the vertical moisture weighted average of the mean WV age, $\Delta\overline{\frac{\{\Lambda\}}{W}}$, and (C) the difference between $\Delta\overline{\frac{\{\Lambda\}}{W}}$ and $\Delta\overline{\nu}$, R_Δ.

Figure 13A presents the relative anomaly of the +2K experiment for the mean age of precipitation. The relative change in ν is very spatially varied, and peaks in magnitude at the poles. Notable increases are located over South America, South Africa and Australia. Clear decreases in ν are located around the west coast of South America, Africa and Northern Australia. For comparaison, the relative anomaly of the +2K experiment for the moisture-weighted, vertically averaged, mean WV age on figure 13B is positive everywhere apart from Eastern Antarctica, the Tibetan plateau and part of the Arctic. $\frac{\langle\{\Lambda\}\rangle}{\langle W\rangle}$'s changes reflect the response of the entire atmospheric column, and the anomaly is therefore smaller and follows the general changes in the moisture transport we saw earlier. Figure 13C presents the relative difference between the change in $\frac{\langle\{\Lambda\}\rangle}{\langle W\rangle}$ and $\langle\nu\rangle$, R_Δ, defined as

$$R_\Delta = \frac{\Delta\overline{\frac{\{\Lambda\}}{W}} - \Delta\overline{\nu}}{\Delta\overline{\frac{\{\Lambda\}}{W}}}. \tag{16}$$

https://doi.org/10.5194/egusphere-2025-6395
Preprint. Discussion started: 23 January 2026
© Author(s) 2026. CC BY 4.0 License.

Regions in red indicate that, in the column above it, the mean WV age has increased by a greater amount than the mean age of the precipitation. On the other hand, regions in blue, indicate that the mean age of precipitation has had a greater change compared to the mean WV age in the column. In the tropics, $R_\Delta > 0$. The average WV age in the column increased due to the increased strength of the Hadley cell. The mean age of precipitation, increased in the tropics, but the magnitude of the response was smaller, since most of the change in WV age happen higher in the updraft, while most of the precipitation happened closer to the surface. In the midlatitudes, $R_\Delta < 0$. The increased eddies increased the mixing, and in turn, the overall mean in the column did not increase by a large amount. On the other hand, the mean age of precipitation increased since the eddies are more sustained, longer and stronger.

Lastly, further analysis of the response of the model to global warming (not shown) indicates that the changes are dominated by the linear response. This is consistent with the linear behaviour of the globally averaged values of mean WV age in figure 8.

4 Discussion

In this study, we developed a set of novel passive tracers to resolve the temporal and spatial variability of the WV age distribution in an Eulerian model. The globally averaged WV age was 7.06 days and the globally averaged precipitation age was 7.33 days. Overall, our method captured the relationship between WV age and the large-scale atmospheric circulation in the control experiment. With climate change, WV age generally increased in the troposphere and decreased in the stratosphere, while the age of precipitation had a very spatially varied response. Globally, mean WV age increased by $4.93\%K^{-1}$ and the age of precipitation increased by 3.16 $\%K^{-1}$. We also showed how WV age's response to climate change is different depending on the region. We were able to simulate the spatial resolution of the change in WV age which could not be previously calculated with indirect methods. Furthermore, there were strong regional difference in the response of WV age and the age of precipitation to climate change. This discrepancy both spatially and globally lies in complex and local processes that we were not able to investigate in the study, but should be the topic of future research.

Our global WV age and age of precipitation estimates fall within the wide range of calculated values, and our locations of maxima and minima generally match the mean lifetime values of Gimeno et al. (2021). The main difference between our mean age of precipitation from figure 7A and Gimeno et al. (2021)'s backward transit time are that we do not have as dominant a maximum over the Sahara, and that we do not have a relative low near the Tibetan plateau. Although the values of ω we calculate roughly match reanalysis over the Sahara (Chen et al., 2014), our model has a very simplified land surface scheme, which creates anomalously high evaporation. Additionally, due to the low resolution of the model, additional moisture from nearby warm oceans can diffuse over the Sahara. Our model does not include snow or ice processess, which may also impact the simulation of water vapor age over the Tibetan plateau. The simplified surface processes may also explain the relatively small value of globally averaged precipitation in our model (Tuinenburg and van der Ent, 2016).

© Author(s) 2026. CC BY 4.0 License.

We also compared our global WV age distribution to previous estimates from Lagrangian experiment by Tuinenburg and van der Ent (2016). At first glance, their calculations do not agree with our results. But, as is detailed in Appendix B, we can recover very similar WV age distributions and age of precipitation maps when we moodify our calculations to match their Lagrangian experiment. Without modification and using a global average over the entire atmosphere, the standard deviation and the tail of our distribution are much greater than the distribution from the 3D-T model they used. This is a great example of how the convention around the results from Lagrangian calculations might differ and in turn induce some confusion when we compare to Eulerian calculations. As mentioned in Table 1, TUT is expected, by its definition, to be equal to the globally averaged mean age of precipitation, which is approximately true in our model, but became incorrect when we focused on the tropics (figure 8). This important discrepancy, in pair with the deviation of our non modified results from the Lagrangian experiment, emphasizes that TUT, mean age of precipitation and mean WV age are not always equivalent, especially when we calculate them with different methods.

In this study, we used the Gamma distribution to estimate the distribution of WV age as was previously done by Tuinenburg and van der Ent (2016). But, previous methods of calculating WV age, either through indirect methods or Lagrangian experiments, did not calculate higher moments of the distribution. Now that we can do so with our WV age distribution moments tracers, we compared the value of the mean, standard deviation and skewness obtained using the moment generating function (MGF, equation 10), to the actual values calculated by the model. The skewness could not be inferred using the MGF. This showed that although the Gamma distribution is a useful way to visualize the WV age distribution, it is not an exact parametrization. But, results from Lagrangian experiments showed good agreement with the Gamma distribution, and, by processing our data in a similar way to theirs we could get similar distributions (see Appendix B). This poses the question: why do the distributions calculated from Lagrangian trajectories limited to 30 days (Tuinenburg and van der Ent, 2016) follow a Gamma distribution, and the moments of the distribution calculated from an Eulerian model do not? Future work should investigate this question inside the maximum entropy methods (Mead and Papanicolaou, 1984).

The reasons why the tracers were implemented on the Isca modeling framework were two-fold. First, it is a very flexible model that permitted us to conduct idealized and realistic experiments. Second, it is cheap to operate and is not as complex as other more sophisticated models. This is good to build our prototype of the tracers and to confirm their worth without exorbitant computing time. But, this does mean that we loose some realism in the simulations. Both the horizontal and vertical resolution were coarse. Also, to accommodate the numerics of our model, we used a hybrid pressure coordinate system that had a very sparse resolution in the troposphere. There was also no ocean parametrization, and no re-evaporation.

In future work, we wish to apply our work to extreme precipitation events. As was previously discussed, we would like to derive the exact parametrization of the WV age distribution using a maximum entropy method to go in depth about the behavior of the WV age distribution. Our work showed the feasibility and value of our WV age tracers, therefore, the next step would be to use them to study the evolution of the water cycle in depth, and to implement them into more complex climate models.

Code and data availability. Code is available on GitHub : https://github.com/PhilippeBoulangerPhysics/Isca. The data from the control and +2K experiment is archived on https://doi.org/10.5683/SP3/U4ZSAZ.

Appendix A: Derivation of the age of a tracer

Consider some tracer c associated with sources and sinks denoted as S^+ and S^-, respectively. In a hydrostatic atmosphere, this tracer as a whole evolves as,[1]

$$\frac{\partial c}{\partial t} + \nabla \cdot \mathbf{v}c = S^+ + S^- = S. \tag{A1}$$

We can perform a simple thought experiment to understand how this can be used to divide a tracer by time of creation. Divide time into N intervals of duration dt starting at 0, so that for the i-th time increment $t_i = i \cdot dt$. At each time step, some tracer amount c_i is injected into the system during the the time interval $[t_i, t_i + dt]$, given by a instantaneous source term S^+. The equation for a tag associated with the instantaneous "pulse" S^+ is (Fajber and Kushner, 2021)

$$\frac{\partial c_i}{\partial t} + \nabla \cdot \mathbf{v}c_i = \frac{c_i}{c} S^- + S^+, \tag{A2}$$

Equation A2 implies that at each time interval, a new tag associated with injection time t_i is initialized between t_i and the next time step. It then evolves/decays like a normal tracer. This allows us to track and evolve the distribution of the tracer c associated with every injection time, and in turn, every age. Since the total amount of tracer generated for each tag is S^+dt, equation A2 implies that $c = \sum_{i=1}^{N} c_i dt$. For a tracer injected into the system at time t_i, the age is given by $a = t - t_i$. If we define the age concentration of the amount of tracer c as c_a so that $c_a da$ is the amount of tracer with age between $(a, a + da)$, then at any given moment in time the amount of tracer associated with that age category is $c_i(t_i = t - a)$, so that we can write

$$c_a da = c_i(t_i = t - a)dt \tag{A3}$$

To find an evolution equation for c_a, we need to consider that at each time step, aging will occur, causing c_a to be associated with the c_i of one time step forward. This means that we can write down the evolution equation for c_a as:

$$\left(\frac{\partial c_a}{\partial t} + \nabla \cdot \mathbf{v}c_a\right) da = \left(\frac{\partial c_i}{\partial t} + \nabla \cdot \mathbf{v}c_i\right) dt + (c_i(t - a + da) - c_i(t - a)) \tag{A4}$$

$$\frac{\partial \tilde{c}}{\partial t} + \nabla \cdot \mathbf{v}\tilde{c} = S^+ + \frac{\tilde{c}}{c} S^- - \frac{\partial \tilde{c}}{\partial a} \tag{A5}$$

where in the last line we have taken the limit as da goes to 0, and used $da/dt = 1$. In this continuous formulation,

$$\lim_{da \to 0} c_a(\mathbf{x}, t) = \tilde{c}(\mathbf{x}, t, a) \quad \text{and} \quad \lim_{da \to 0} \sum_{a=0}^{N \cdot dt} da = \int_0^t \cdot da. \tag{A6}$$

---

[1] The horizontal diffusion term was ignored, but the following discussion works for any linear differential operator.

Directly implementing this type of tracer that tracks the entire distribution of ages requires initializing new tags at every time step and is very computationally expensive. To circumvent this issue, we will derive the evolution equation of the normalized moments of the distribution. The discrete formulation of the n-th normalized moment is

$$\mu_n(t,\boldsymbol{x}) = \frac{1}{c}\int\limits_0^\infty a^n \tilde{c}\, da. \tag{A7}$$

By multiplying equation A7 by c and applying a material derivative, we arrive at

$$c\left(\frac{\partial}{\partial t} + \nabla\cdot\mathbf{v}\right)\mu_n + \mu_n\left(\frac{\partial}{\partial t} + \nabla\cdot\mathbf{v}\right)c = \int\limits_0^\infty a^n\left(S^+ + \frac{\tilde{c}}{c}S^- - \frac{\partial\tilde{c}}{\partial a}\right)da. \tag{A8}$$

The left-hand side of equation A8 can be simplified using equation A1,

$$c\left(\frac{\partial}{\partial t} + \nabla\cdot\mathbf{v}\right)\mu_n + \mu_n\left(\frac{\partial}{\partial t} + \nabla\cdot\mathbf{v}\right)c = c\left(\frac{\partial}{\partial t} + \nabla\cdot\mathbf{v}\right)\mu_n + \mu_n\left(S^+ + S^-\right).$$

The right-hand side can be simplified into

$$\int\limits_0^\infty a^n\left(\frac{\tilde{c}}{c}S^- + S^+ - \frac{\partial\tilde{c}}{\partial a}\right)da = \mu_n S^- + S^+(t=t_j)a(t=t_j) - \int\limits_0^\infty a^n\left(\frac{\partial\tilde{c}}{\partial a}\right)da. \tag{A9}$$

The first term can be simplified into the n-th normalized moment. The instantaneous source term is non-zero at the time of injection, where the age is equal to 0, so the second term on the RHS vanishes in equation A9. Therefore, we arrive at this intermediate formulation of the moments evolution equation,

$$c\left(\frac{\partial}{\partial t} + \nabla\cdot\mathbf{v}\right)\mu_n + \mu_n\left(S^+ + S^-\right) = \mu_n S^- - \int\limits_0^\infty a^n\left(\frac{\partial\tilde{c}}{\partial a}\right)da, \tag{A10}$$

where $a(t=t_i) = 0$ and $\tilde{c} > 0$. The last term on the right-hand side is simplified by integrating by parts,

$$-\int\limits_0^\infty a^n\frac{\partial\tilde{c}}{\partial a}da = -\left(a^n\tilde{c}\right)\big|_0^\infty + \int\limits_0^\infty n a^{n-1}\frac{\tilde{c}}{c}da = \int\limits_0^\infty n a^{n-1}\frac{\tilde{c}}{c}da = n\mu_{n-1}, \tag{A11}$$

So, our final expression for the evolution equation of the n-th moment of the age distribution is

$$\left(\frac{\partial}{\partial t} + \nabla\cdot\mathbf{v}\right)\mu_n = n\mu_{n-1} - \frac{S^+}{c}\mu_n, \tag{A12}$$

where $\mu_0 = 1$. Alternatively, this equation can be written as

$$\left(\frac{\partial}{\partial t} + \nabla\cdot\mathbf{v}\right)(c\mu_n) = nc\mu_{n-1} + S^- c\mu_n. \tag{A13}$$

Equation A12 and A13 can be used to directly calculate the age of a given tracer in a GCM. One only needs to gather the sources or sinks at each time step to incorporate this tool into their model. By applying this theory to water vapor, we can track the moments of the WV age distribution in a GCM, and in turn, spatially resolve the mean WV age as well as any other moments of the distribution.

Appendix B: Comparison with Lagrangian experiment

Tuinenburg and van der Ent (2016) calculated the distribution of WV age with trajectories with the 3D-T (Tuinenburg, 2013) and WAM-2layers model. In this study, WV was tracked for 30 days along its trajectory to calculate its age. Any moisture left after 30 days was considered to have the fixed age of 30 days. Then, to get global values, the PDFs were summed for all time steps, weighted by the amount of evaporation during the time of release. For global averages, data from the WAM-2layers models above ±80° were excluded. All in all, they calculated 3 metrics, the residence time of precipitation, the age of evaporation and the age of atmospheric WV. Based on their description of these metrics, they correspond to age of precipitation, forward transit time (FTT) and WV age respectivly. We were able to compare their maps of age of precipitation and age of atmospheric WV, as well as their global distribution of FTT with our data.

A key difference between their approach and ours is that our mean WV age is not limited to 30 days, so the tails of our distribution should be greater, and the overall shape of the distribution should be different. Therefore, to better compare the 2 distributions, we modify our spatial resolution of the first and second moments in the following manner. Any point where the addition of the mean age and one standard deviation is greater than 30 days gets set to this value. The PDF collapsed to one singular value. Therefore, the second moment gets set to $\mu_2 = \sqrt{\mu_1}$ so that the standard deviation is 0. The time average is weighted by the amount of evaporation in this time step.

With figure B1, we can compare the residence time of precipitation and age of atmospheric water vapor from Tuinenburg and van der Ent (2016) to our values of modified values of ν and $\frac{\langle\{\Lambda\}\rangle}{\langle W\rangle}$. The mean residence time or age of precipitation, (figures B1A and B1C) is consistently lower in our calculation versus the Lagrangian experiment. The most important difference is over land, where ν does not increase compared to the ocean, and is much lower than the residence time of precipitation. But, over the ocean, we can see how the spatial distribution coincides with each other. The local maxima and minima in the Pacific ocean align very well. Over the Sahara, ν is lower than the residence time of precipitation. As previously explained in section 3.1 and discussed in section 4, our non-realistic land parametrization can explain the difference between figures B1A and B1C over the land. Over the ocean, we do have comparable patterns. This is positive and seems to indicate that our WV age tracers indeed follow WV transport realistically. Again, we also have a coarse resolution, especially compared to the 0.25°×0.25° of the Lagrangian experiment. Therefore, the pattern of the dynamics can slightly differ. Globally, the residence time of precipitation is 8.45 days, more than a day greater than our $\overline{\langle\nu\rangle} = 7.33$ days.

The vertically integrated mean WV age also has a similar spatial pattern to the age of atmospheric water, but with a smaller magnitude. Some of the deviation is due to the land parametrization we just discussed. Other could be due to the resolution discrepancy. But, we feel that, overall, we can get similar results to the Lagrangian experiments. Globally, the age of atmospheric WV is 7.88 days, which is fairly close to our value of 7.06 days for $\overline{\frac{\langle\{\Lambda\}\rangle}{\langle W\rangle}}$.

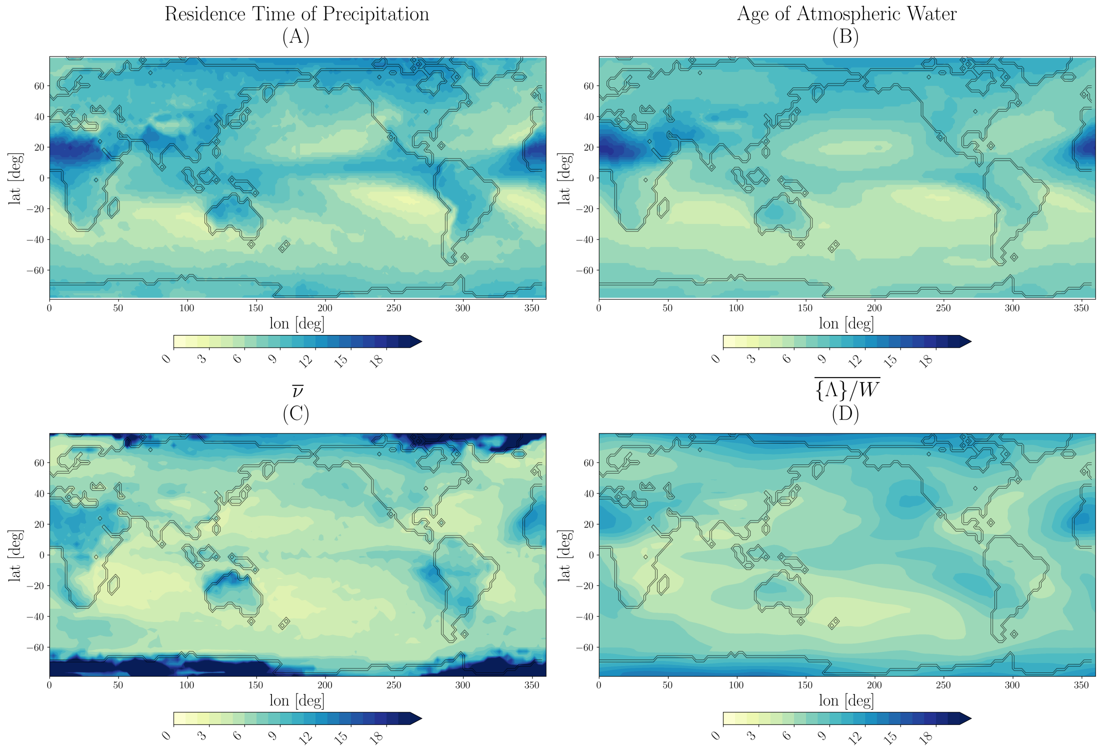

Figure B1. Time average of (A) the residence time of precipitation, and (B) the age of atmospheric water vapor from Tuinenburg and van der Ent (2016). Also, the time average of (C) the modified mean age of precipitation, $\overline{\nu}$, (D) the vertical moisture weighted average of the modified mean WV age, $\overline{\frac{\{\Lambda\}}{W}}$. In our data, any point where the addition of the mean age and one standard deviation was greater than 30 days got set to this value, the second moment got set to $\mu_2 = \mu_1$.

Since FTT should be, on average, equal to BTT (see Table 2). We can use the available global FTT distribution to compare to our globally averaged WV age distribution. Figure B2 presents the distribution of age of evaporation from Tuinenburg and van der Ent (2016) obtained from the 3D-T model, its fit, and the Gamma distribution obtained from the first 2 moment tracers, both the (A) modified and (B) not modified versions of it. Since the sample distribution uses data from the 3D-T model, the global average extends to the entire globe, contrary to the previous global averages. When we comply to the assumptions imposed by the Lagrangian experiment, we arrive at a distribution that is somewhat close to Tuinenburg and van der Ent (2016) (figure B2). Without modification and using a global average over the entire atmosphere, the standard deviation and the tail of our distribution are much greater than the distribution from the 3D-T model.

Author contributions. Prof. Robert Fajber conceptualized the study, designed the methodology and edited the manuscript. Philippe Boulanger implemented the tracers in the climate model, ran the simulation, analyzed the data and drafted the manuscript.

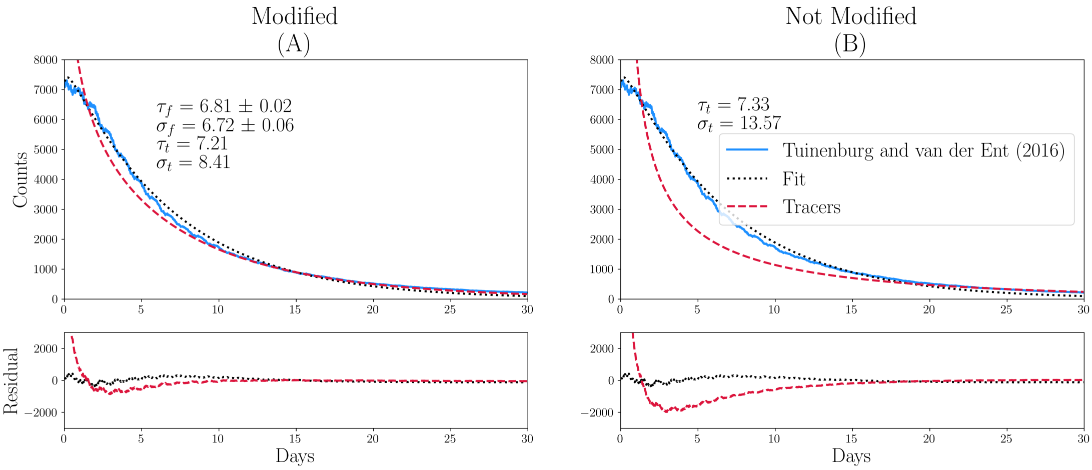

Figure B2. The distribution of age of evaporation from Tuinenburg and van der Ent (2016) obtained from the 3D-T model, its fit, and the Gamma distribution obtained from the first 2 moment tracers, from (A) modified and (B) non modified datasets.

Competing interests. The authors declare that they have no conflict of interest.

Acknowledgements. This research was supported by the HAWC mission (High altitude Aerosol Water vapor and Clouds) and the BRACE Water Center. The authors would like to thank Ruud J, van der Ent for providing comparison data.

References

Allan, R. P., Barlow, M., Byrne, M. P., Cherchi, A., Douville, H., Fowler, H. J., Gan, T. Y., Pendergrass, A. G., Rosenfeld, D., Swann, A. L. S., Wilcox, L. J., and Zolina, O.: Advances in understanding large-scale responses of the water cycle to climate change, Annals of the New York Academy of Sciences, 1472, 49–75, https://doi.org/https://doi.org/10.1111/nyas.14337, 2020.

Ayantobo, O. O. and Wei, J.: Quantifying Climate-Induced Changes in the Tibetan Plateau's Hydrologic Cycle Through Atmospheric Moisture Depletion and Restoration Times, Water Resources Research, 61, e2024WR037 644, https://doi.org/https://doi.org/10.1029/2024WR037644, 2025.

Betts, A. K.: A new convective adjustment scheme. Part I: Observational and theoretical basis, Quarterly Journal of the Royal Meteorological Society, 112, 677–691, https://doi.org/10.1002/qj.49711247307, 1986.

Bonan, D. B., Schneider, T., and Zhu, J.: Precipitation Over a Wide Range of Climates Simulated With Comprehensive GCMs, Geophysical Research Letters, 51, e2024GL109 892, https://doi.org/https://doi.org/10.1029/2024GL109892, 2024.

Byrne, M. P., Pendergrass, A. G., Rapp, A. D., and Wodzicki, K. R.: Response of the Intertropical Convergence Zone to Climate Change: Location, Width, and Strength, Current Climate Change Reports, 4, 355–370, https://doi.org/10.1007/s40641-018-0110-5, 2018.

Chen, S., Wei, K., Chen, W., and Song, L.: Regional changes in the annual mean Hadley circulation in recent decades, Journal of Geophysical Research: Atmospheres, 119, 7815–7832, https://doi.org/https://doi.org/10.1002/2014JD021540, 2014.

Dessler, A. E., Hintsa, E. J., Weinstock, E. M., Anderson, J. G., and Chan, K. R.: Mechanisms controlling water vapor in the lower stratosphere: "A tale of two stratospheres", Journal of Geophysical Research: Atmospheres, 100, 23 167–23 172, https://doi.org/https://doi.org/10.1029/95JD02455, 1995.

Fajber, R. and Kushner, P. J.: Using 'Heat Tagging' to Understand the Remote Influence of Atmospheric Diabatic Heating through Long-Range Transport, Journal of the Atmospheric Sciences, 78, 2161–2174, https://doi.org/10.1175/JAS-D-20-0290.1, 2021.

Fajber, R., Kushner, P. J., and Laliberté, F.: Influence of Midlatitude Surface Thermal Anomalies on the Polar Midtroposphere in an Idealized Moist Model, Journal of the Atmospheric Sciences, 75, 1089 – 1104, https://doi.org/10.1175/JAS-D-17-0283.1, 2018.

Frierson, D. M. W.: The Dynamics of Idealized Convection Schemes and Their Effect on the Zonally Averaged Tropical Circulation, Journal of the Atmospheric Sciences, 64, 1959 – 1976, https://doi.org/10.1175/JAS3935.1, 2007.

Frierson, D. M. W., Held, I. M., and Zurita-Gotor, P.: A Gray-Radiation Aquaplanet Moist GCM. Part I: Static Stability and Eddy Scale, Journal of the Atmospheric Sciences, 63, 2548 – 2566, https://doi.org/10.1175/JAS3753.1, 2006.

Frierson, D. M. W., Lu, J., and Chen, G.: Width of the Hadley cell in simple and comprehensive general circulation models, Geophysical Research Letters, 34, https://doi.org/https://doi.org/10.1029/2007GL031115, 2007.

Galewsky, J., Sobel, A., and Held, I.: Diagnosis of Subtropical Humidity Dynamics Using Tracers of Last Saturation, Journal of the Atmospheric Sciences, 62, 3353 – 3367, https://doi.org/10.1175/JAS3533.1, 2005.

Gimeno, L., Eiras-Barca, J., Durán-Quesada, A. M., Dominguez, F., van der Ent, R., Sodemann, H., Sánchez-Murillo, R., Nieto, R., and Kirchner, J. W.: The residence time of water vapour in the atmosphere, Nature Reviews Earth & Environment, 2, 558–569, 2021.

Hall, T. M. and Plumb, R. A.: Age as a diagnostic of stratospheric transport, Journal of Geophysical Research: Atmospheres, 99, 1059–1070, https://doi.org/https://doi.org/10.1029/93JD03192, 1994.

Held, I. M. and Soden, B. J.: Robust Responses of the Hydrological Cycle to Global Warming, Journal of Climate, 19, 5686 – 5699, https://doi.org/10.1175/JCLI3990.1, 2006.

Holton, J. R., Haynes, P. H., McIntyre, M. E., Douglass, A. R., Rood, R. B., and Pfister, L.: Stratosphere-troposphere exchange, Reviews of Geophysics, 33, 403–439, https://doi.org/https://doi.org/10.1029/95RG02097, 1995.

Holzer, M. and Boer, G. J.: Simulated Changes in Atmospheric Transport Climate, Journal of Climate, 14, 4398 – 4420, https://doi.org/10.1175/1520-0442(2001)014<4398:SCIATC>2.0.CO;2, 2001.

Langille, J., Bourassa, A., Pan, L. L., Letros, D., Solheim, B., Zawada, D., and Degenstein, D.: Observational evidence of moistening the lowermost stratosphere via isentropic mixing across the subtropical jet, Atmospheric Chemistry and Physics, 20, 5477–5486, https://doi.org/10.5194/acp-20-5477-2020, 2020.

Lutsko, N. J., Martinez-Claros, J., and Koll, D. D. B.: Atmospheric Moisture Decreases Midlatitude Eddy Kinetic Energy, Journal of the Atmospheric Sciences, 81, 1817 – 1832, https://doi.org/10.1175/JAS-D-23-0226.1, 2024.

Läderach, A. and Sodemann, H.: A revised picture of the atmospheric moisture residence time, Geophysical Research Letters, 43, 924–933, https://doi.org/https://doi.org/10.1002/2015GL067449, 2016.

Manabe, S.: Climate and the ocean circulation, 1. The atmospheric circulation and the hydrology of the Earth's surface, Monthly Weather Review, 97, 739–774, https://doi.org/10.1175/1520-0493(1969)097<0739:CATOCT>2.3.CO;2, 1969.

Mead, L. R. and Papanicolaou, N.: Maximum entropy in the problem of moments, Journal of Mathematical Physics, 25, 2404–2417, https://doi.org/10.1063/1.526446, *Received* 8 November 1983; *Accepted* 13 January 1984, 1984.

Mlawer, E. J., Taubman, S. J., Brown, P. D., Iacono, M. J., and Clough, S. A.: Radiative transfer for inhomogeneous atmospheres: RRTM, a validated correlated-k model for the longwave, Journal of Geophysical Research: Atmospheres, 102, 16 663–16 682, https://doi.org/10.1029/97JD00237, 1997.

Nieto, R. and Gimeno, L.: A database of optimal integration times for Lagrangian studies of atmospheric moisture sources and sinks, Scientific Data, 6, 59, https://doi.org/10.1038/s41597-019-0068-8, 2019.

Numaguti, A.: Origin and recycling processes of precipitating water over the Eurasian continent: Experiments using an atmospheric general circulation model, Journal of Geophysical Research: Atmospheres, 104, 1957–1972, https://doi.org/https://doi.org/10.1029/1998JD200026, 1999.

Orbe, C., Waugh, D. W., Newman, P. A., and Steenrod, S.: The Transit-Time Distribution from the Northern Hemisphere Midlatitude Surface, Journal of the Atmospheric Sciences, 73, 3785 – 3802, 2016.

O'Gorman, P. A. and Schneider, T.: The Hydrological Cycle over a Wide Range of Climates Simulated with an Idealized GCM, Journal of Climate, 21, 3815 – 3832, https://doi.org/10.1175/2007JCLI2065.1, 2008.

Pendergrass, A. G.: The Global-Mean Precipitation Response to CO2-Induced Warming in CMIP6 Models, Geophysical Research Letters, 47, e2020GL089 964, https://doi.org/https://doi.org/10.1029/2020GL089964, 2020.

Seager, R., Naik, N., and Vecchi, G. A.: Thermodynamic and Dynamic Mechanisms for Large-Scale Changes in the Hydrological Cycle in Response to Global Warming, Journal of Climate, 23, 4651 – 4668, https://doi.org/10.1175/2010JCLI3655.1, 2010.

Sodemann, H.: Beyond Turnover Time: Constraining the Lifetime Distribution of Water Vapor from Simple and Complex Approaches, Journal of the Atmospheric Sciences, 77, 413 – 433, https://doi.org/10.1175/JAS-D-18-0336.1, 2020.

Trenberth, K.: Changes in Precipitation with Climate Change. Climate Change Research, Climate Research, 47, 123–138, https://doi.org/10.3354/cr00953, 2011.

Trenberth, K. E.: Atmospheric Moisture Residence Times and Cycling: Implications for Rainfall Rates and Climate Change, Climatic Change, 39, 667–694, https://doi.org/10.1023/A:1005319109110, 1998.

© Author(s) 2026. CC BY 4.0 License.

Trenberth, K. E. and Stepaniak, D. P.: Seamless Poleward Atmospheric Energy Transports and Implications for the Hadley Circulation, Journal of Climate, 16, 3706 – 3722, https://doi.org/10.1175/1520-0442(2003)016<3706:SPAETA>2.0.CO;2, 2003.

Tuinenburg, O. A.: Atmospheric Effects of Irrigation in Monsoon Climate: The Indian Subcontinent, http://edepot.wur.nl/254036, last accessed: 23 November 2016, 2013.

Tuinenburg, O. A. and van der Ent, R. J.: The residence time of water in the atmosphere revisited, Hydrology and Earth System Sciences Discussions, pp. 1–15, https://doi.org/10.5194/hess-2016-431, 2016.

Tuinenburg, O. A. and van der Ent, R. J.: Land Surface Processes Create Patterns in Atmospheric Residence Time of Water, JGR Atmospheres, 124, 583–600, https://doi.org/10.1029/2018JD028871, open Access, 2019.

Vallis, G. K., Zurita-Gotor, P., Cairns, C., and Kidston, J.: Response of the large-scale structure of the atmosphere to global warming, Quarterly Journal of the Royal Meteorological Society, 141, 1479–1501, https://doi.org/https://doi.org/10.1002/qj.2456, 2015.

Vallis, G. K., Colyer, G., Geen, R., Gerber, E., Jucker, M., Maher, P., Paterson, A., Pietschnig, M., Penn, J., and Thomson, S. I.: Isca, v1.0: a framework for the global modelling of the atmospheres of Earth and other planets at varying levels of complexity, Geoscientific Model Development, 11, 843–859, https://doi.org/10.5194/gmd-11-843-2018, 2018.

Wang-Erlandsson, L., van der Ent, R. J., Gordon, L. J., and Savenije, H. H. G.: Contrasting roles of interception and transpiration in the hydrological cycle ndash; Part 1: Temporal characteristics over land, Earth System Dynamics, 5, 441–469, https://doi.org/10.5194/esd-5-441-2014, 2014.

Waugh, D. and Hall, T.: AGE OF STRATOSPHERIC AIR: THEORY, OBSERVATIONS, AND MODELS, Reviews of Geophysics, 40, 1–1–1–26, https://doi.org/https://doi.org/10.1029/2000RG000101, 2002.

Wu, Y. and Pauluis, O.: Examination of Isentropic Circulation Response to a Doubling of Carbon Dioxide Using Statistical Transformed Eulerian Mean, Journal of the Atmospheric Sciences, 70, 1649 – 1667, https://doi.org/10.1175/JAS-D-12-0235.1, 2013.

Éric J.M Delhez and Éric Deleersnijder: The concept of age in marine modelling: II. Concentration distribution function in the English Channel and the North Sea, Journal of Marine Systems, 31, 279–297, https://doi.org/https://doi.org/10.1016/S0924-7963(01)00066-5, 2002.